RPC-ICA User Guide

General Information

Contact:
Hans Nilsson, Swedish Institute of Space Physics, Kiruna, Sweden
Email: hans.nilsson@irf.se

Covers RPC-ICA PSA data L2, L3, L4 CORR and L4 PHYS-MASS, L5 moments

Revision 1.5 of 20210216

Table of Contents

Scope

The scope of this guide is to show how RPC-ICA data can be used. It is assumed that the user can read the data from the PDS formatted data files. The format is only very briefly described in this User Guide. For details on the format the user is referred to the Experimenter to Archive Interface Control Document and the PSA data labels. The format is also described briefly in Appendix A.

The instrument paper (Nilsson et al. 2007) is somewhat outdated, an update on the instrument characteristics compared to that document is provided.

Conventions

The instrument has 16 directional anodes, termed sectors. The angle of the field of view of a sector is referred to as the azimuthal angle. Sectors are numbered from 0, i.e. 0 to 15.
There are likewise 16 elevation steps, corresponding to the angle of the look direction out of the detector symmetry plane. We refer to this angle as the elevation angle. Elevations are numbered from 0, i.e. 0 to 15.
There are 32 mass anodes, termed mass channels in our text. These are numbered from 0, i.e. 0-31.
To be consistent with the naming scheme of sectors, elevations and mass channels, whenever we refer to the index of a variable, we start from 0.

Introduction

RPC-ICA is a mass resolving ion spectrometer on-board the Rosetta spacecraft. It is a part of the Rosetta Plasma Consortium (Carr et al. 2007) which also consists of the RPC-IES ion and electron spectrometer (Burch et al. 2007), the RPC-MAG magnetometer (Glassmeier et al. 2007), the RPC-LAP Langmuir probe (Eriksson et al. 2007) and the RPC-MIP Mutual Impedance Probe (Trotignon et al. 2007).

RPC-ICA has limited mass resolution and an about 2 pi angular coverage and can measure positively charged ions in an energy range from a few eV to 40 keV. The instrument is described in Nilsson et al. (2007), though some of the information there is out of date. Further updates regarding the energy scale has been published in Nilsson et al. (2015a,b) and concerning a temperature drift in Nilsson et al. (2017). An updated instrument summary is given in section Instrument characteristics. A new way of operating the instrument using a restricted energy range and two-dimensional data provides much improved temporal resolution. This data is described further in Stenberg Wieser et al. (2017).

The data from the first encounter of Rosetta with the comet atmosphere was published in Nilsson et al. (2015a). A brief summary of the RPC-ICA data from

the full mission was given in Nilsson et al. (2017) while a summary of how the comet ionosphere affected the solar wind throughout the mission was given in Behar et al. (2017). The effect of the neutral atmosphere, manifested as a presence of He^+ ions formed through charge exchange of solar wind He^{2+} with atmospheric constituents (mainly H_2O) was given in Simon Wedlund et al. (2016). Some further examples of studied science problems can be found in the RPC User Guide.

Instrument Characteristics

The main change in the instrument characteristics as compared to what was given in the instrument paper (Nilsson et al. 2007) is that the lower energy threshold is now determined to be a few eV while it was given as 25 eV in the instrument paper. A new way of operating the instrument giving two-dimensional data with high time resolution was implemented in-flight (Stenberg Wieser et al. 2017).

Upon encounter with the cometary environment, it was discovered that the RPC-ICA voltages of the electrostatic analyser differed considerably from what they were expected to be. The same thing happened to the twin instrument IMA, part of ASPERA-3 on Mars Express. The data delivered to the ESA PSA archive has been corrected for this, but the early data, from before corrected tables were uploaded, have rather coarse sampling of the low energy ion populations. The new tables were in use from 30 October 2014. Therefore, for most purposes it is better to use data from then or later when studying cometary ions. The improved energy tables were used in software versions 4 and higher. The elevation tables were also updated. The early data suffered from coarser than needed angular sampling due to the mismatch between expected and actual energy. The on-board mass lookup tables were not updated at first, so that at low energies the nominal mass ranges which data were binned in did not correspond to the expected physical ion mass ranges. This was fixed from software version 9. The archive data, also the data binned using on-board mass lookup tables, has been expanded to the original 32 mass channels. For most purposes except subdivision of cometary ions into subgroups (water group and CO_2 and similar mass) the Normal mode data using on-board mass lookup tables can be used, see further discussion in section Mass Separation.

The RPC-ICA instrument also suffered from failed decompression of the on-board loss-less compressed data. It was later found out that this was at least partly because of a packet loss between RPC-ICA and the central Plasma Interface Unit. This loss did not occur in the much binned lower telemetry rate Normal mode data. Once it was found that it did not occur in the high angular resolution instrument modes (which bins mass channels at least two and two), the latter mode was used most of the time. Towards the end of the mission a software version (10) was tested with an increased delay time between data packets, and this appeared to solve the problem of lost packets. It also turned out to lower the telemetry rate so this software version was not much used. The data loss due to failed decompression was significant and makes all RPC-ICA data in burst mode, from start of mission until approximately June 2015, rather patchy. After the

discovery that high angular resolution burst mode data could be used without data loss, the high mass resolution mode was still used for part of the time, to allow for a cross-comparison between the higher and lower mass resolution data.

Another problem for the RPC-ICA instrument during the early part of the mission was sudden overheating of the instrument, which led to automatic switch off. The sensor showing increased temperatures was glued onto an FPGA circuit, so a latch-up in the FPGA was suspected. As this could lead to permanent damage the instrument was initially used rather seldom and for short periods. After a while the overheating events disappeared and from mid December 2014 the instrument was run essentially all the time, except for time periods during and after thruster firings.

The instrument characteristics are summarized in table 1.

Table 1 Instrument characteristics

Quantity		**Range**
Energy	Range	Few eV to 40 keV
	Resolution	$\Delta E/E = 0.07$
	Scan	8, 32 or 96 steps
Angle	Range	90° x 360° (about 2 pi sr free view)
	Resolution	5.0° x 22.5° (16 elevation steps x 16 sectors)
Temporal resolution	2D distribution	1 s, 4 s or 12 s
	3D distribution	192 s

ICA Data description

The different data sets in PSA

There are 4 different data sets delivered to PSA as described in table 2.

Table 2 The ICA data sets in PSA

Data set name	Type of data	Use
L2	Raw data [counts]	The original data, the goal was to make the data set complete. Best starting point when users need to apply their own noise reduction methods or look at very weak signals applying their own statistical methods.
L3	Calibrated data in reversible format [differential flux]	The L2 data with just calibration constants applied
L4 CORR CTS	Raw data irreversibly treated for cross-talk and noise treatment [counts]	Raw data where the noise removal has been taken into account and cross talk treated in an automatic manner. May look noisier than original data. Useful for statistical studies, studies of weak signals and similar. Useful for user defined noise suppression. Also for separating heavier ions into subgroups (water group and CO_2 group).
L4 CORR	Calibrated data irreversibly treated for cross-talk and noise treatment [differential flux]	Calibrated data where the noise removal has been taken into account and cross talk treated in an automatic manner. May look noisier than original data. Useful for statistical studies, studies of weak signals and similar. Also for separating heavier ions into subgroups (water group and CO_2 group).
L4 PHYS_MASS	Data separated into 4 physical ion mass	The easiest to use data set, separated into 4 ion mass

	ranges, with conservative noise and cross-talk suppression [differential flux]	ranges (H^+, He^{2+}, He^+ and heavy ions corresponding to a molecular weight of oxygen and higher). Weak signals may have been removed by noise suppression. Cross-talk between light and heavy ion mass channels suppressed in conservative manner, possibly removing some real data.

Data treatment in L4 CORR

The data delivered in the data set L4 CORR has been treated by an automatic algorithm that step by step attempts to remove a number of artefacts from the data. Figure 1 shows an example from 2016-02-24 at 18:00 UT.

First a background noise removal can be performed. It is a removal of single data points with all neighbours being zero. This is illustrated by the difference between the upper row of figure 1 and the second row. The different columns show data summed over all variables except those indicated on the axis. Column 1 shows sector and energy, column 2 mass channel and energy, column 3 sector and elevation, and column 4 mass channel and sector. The noise treatment also takes the on-board noise subtraction into account, trying to adjust for its effect.

The next step makes the mass response of the different mass channels smoother and attempts to remove cross talk between mass channels (row 3).

Thereafter an attempt is made to identify broadening of strong signals, which spill over on neighbouring mass channels. The broad signal seen over many (mostly all) mass channels is often referred to as a ghost (row 4). Row 5 shows the identified broadened signal that was removed.

Finally sector cross-talk is remedied.

The corrections are not perfect, sectors prone to pick up cross-talk may still contain erroneous signal. The data set contains an additional way to identify uncertain data. In the PSA data set there is also a ZERO file delivered together with the data. It contains a value which is an uncertainty estimate of the zero level. Data less than this value cannot be considered different from zero. Sectors and mass channels from which a lot of cross talk has been removed have larger uncertainties.
As subtractions have been performed, the data may be less than zero. If desired, data less than zero can be set to zero, but only after all desired binning or summing of the data has been made, to assure best possible statistical accuracy.

Rows 2 – 6 of figure 1 show only positive data values. All negative data values are shown in dark blue independent of the actual value. Correspondingly, the bottom

4 rows of figure 1 show only negative data values, all positive values are replaced by dark blue. Ideally, there should be no negative data values, but statistical noise and non-ideal corrections will result in some negative data values. If the magnitude of the negative values exceeds the numbers given in the ZERO file, care should be taken when interpreting the data.

The above corrections cannot always be used if the data is strongly binned onboard (which is done in order to reduce the required telemetry rate), se next section.

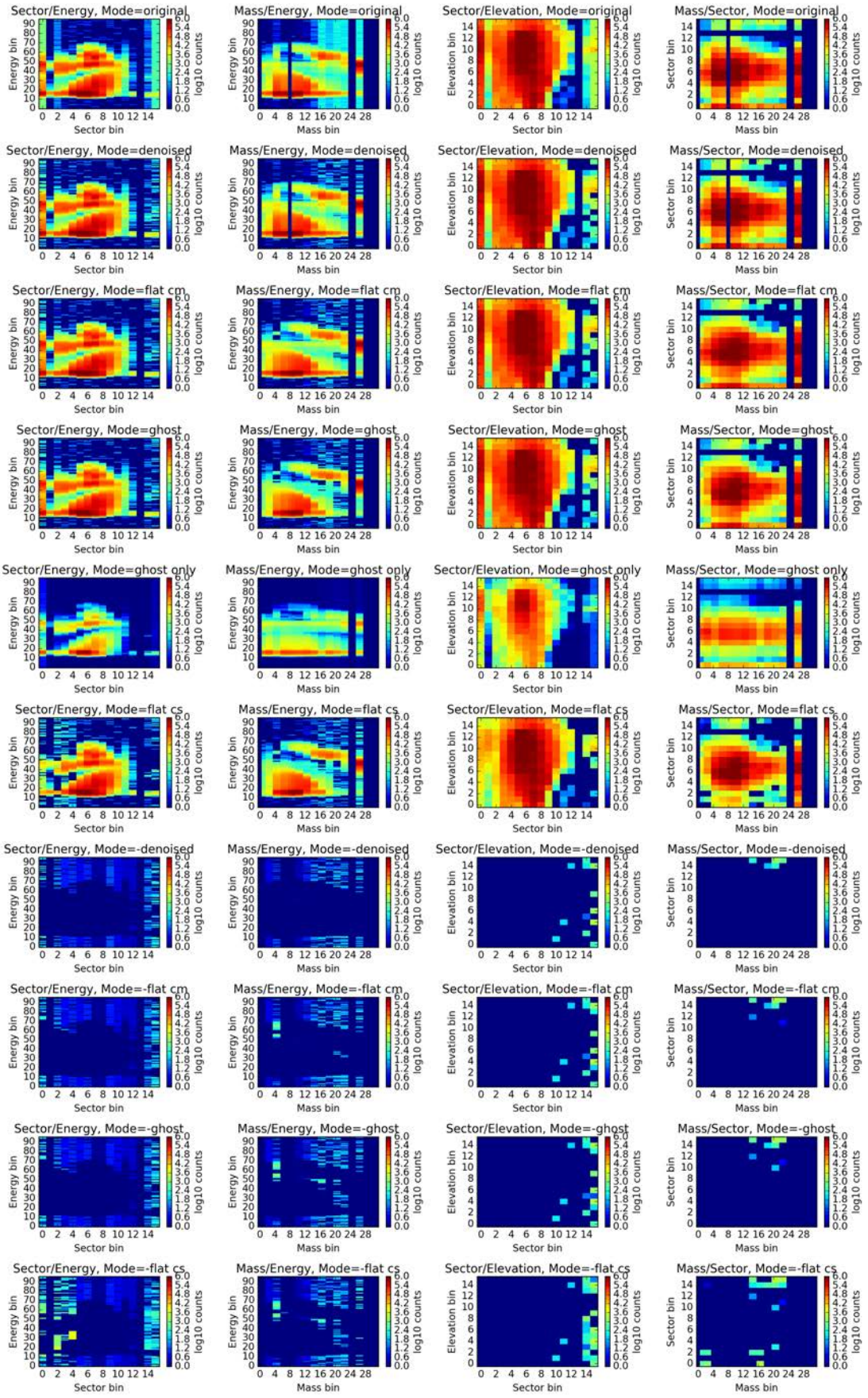

Figure 1 L4 CORR data correction steps.

What the data contains

The RPC-ICA PDS files all contain one energy spectrogram per line, with additional information about the time of the observations, length of the observation, quality flags, instrument mode, level of on-board noise reduction, mass table used, post acceleration level, azimuth (sector), elevation and mass channel for the particular energy spectra. The data layout is summarized in Appendix 1. We will here briefly describe what these variables mean and how they can be used.

The azimuth and elevation provide the look direction of the instrument. The physical azimuth (sector) angle corresponding to a given azimuth index (0-15) is constant in the instrument frame. See section "Working with geometry data" for more information about physical angles. The elevation angle corresponding to a given index value (0-15) varies with energy and software version and is given in an elevation table provided with the data. It is recommended that the user read all elevation tables into a multidimensional variable being a function of software version, energy and elevation index.

The mass channel (0-31) corresponds to the radius at which a particle hits the detector surface. Lighter and lower energy particles hit the detector at a larger radius and thus higher mass channel number. Heavier and more energetic particles hit the detector at a smaller radius. The post acceleration level indicates the degree of acceleration of particles between the energy acceptance filter and the magnetic momentum filter, thus also affecting where particles of a given energy and mass will hit the detector. At what mass channels particles of a given mass and energy hit the detector is discussed in section "Mass separation".

In order to stay within available telemetry limits data was binned on-board. How it was binned is given by table 3. The default operating mode was that the instrument automatically adjusted the binning to stay within telemetry limits, thus changing the instrument "mode".

Table 3 The ICA instrument modes

Mode	Index	Masses	Azimuth angles	Energies	Elevation angles
NRM-0	8	6	16	96	16
NRM-1	9	6	16	96	8
NRM-2	10	6	16	96	4
NRM-3	11	6	16	96	2
NRM-4	12	6	8	96	2
NRM-5	13	6	4	96	2
NRM-6	14	3	4	96	2
NRM-7	15	3	4	96	1
HAR-0	16	16	16	96	16
HAR-1	17	16	16	96	8
HAR-2	18	16	16	96	4
HAR-3	19	8	16	96	4
HAR-4	20	4	16	96	4
HAR-5	21	2	16	96	4
HAR-6	22	2	8	96	4
HAR-7	23	2	8	96	4
EXM-0	24	32	16	96	16
EXM-1	25	32	16	96	8
EXM-2	26	32	16	96	4
EXM-3	27	32	16	96	2
EXM-4	28	32	8	96	2
EXM-5	29	32	4	96	2
EXM-6	30	32	2	96	2
EXM-7	31	32	2	96	1

The Normal modes (NRM) were designed for normal mode telemetry rates of 100 bits/s and use on-board lookup tables for the mass binning. High Angular Resolution (HAR) burst modes (designed for 1 kbit/s data rate) give priority to angular resolution, whereas EXM modes give priority to mass resolution. For certain scientific questions it may be necessary to put a demand on the data that it is within a range of mode numbers to give sufficient angular or mass resolution.

To make on-board loss-less data compression more efficient an on-board noise reduction was frequently used. The value was typically set to 2, meaning that 2 was subtracted from each data point, after binning. Data being less than 0 after subtraction was set to 0. Data with no background subtraction looks much more noisy but is fine to use. The enhanced archive L4 CORR data has a background noise treatment that attempts to even out the effect of the background noise reduction.

The high time resolution data does not fit into the instrument mode scheme. Apart from a period in May 2015 the high time resolution data was obtained in mode 16, HAR-0. The automatic binning to stay within available telemetry was turned off. This can lead to data gaps instead. The reason for this is that if

different elevations are binned together, then data 12 s apart will be binned together. This did happen for some data in May 2015, a quality flag warns for this. The elevation index of high time resolution data goes between 0 and 15 just as for 3D data, repeated 3 or 12 times for 4 s and 1 s resolution data respectively. This reflects the fact that high time resolution data uses a sawtooth-patterned energy scale and constant elevation, but internally to the instrument it works the same way as the 3D data.

For the L5 moment data, which is a combination of data with higher time resolution, the flag is the maximum of the flags of all data contributing to the moment calculation.

The 8 quality flags of the data are described in the EAICD, and also given below.

1. Field of view blocked by the spacecraft. Certain sector and elevation combinations look into the spacecraft. These are flagged here. This flag is not relevant for the L5 (moment) data.
2. Inappropriate instrument mode used with software version 7 or 8. Such data do not have as high time resolution as indicated as spectrograms 12 s or more apart has been added together.
3. Low instrument temperature
4. Enhanced background noise
5. Quality of solar wind cross talk removal. Not implemented for L2/L3
6. Extraordinary data of uncertain nature. Not implemented for L2/L3
7. ICA-LAP correlation flag.
8. Spare

All flags are such that 0 indicates no known problem, X means not implemented for this data set and a non-zero number indicates progressively worse problems or for the Extraordinary data flag a number that identifies a known type of data, described in more detail in section “Strange signals in the data”.
Flag position 7 indicates whether there is good correlation between the RPC-ICA ion flux and the ion current and spacecraft potential. In order to be consistent with the other flags, 0 means good correlation with RPC-LAP ion current and spacecraft potential, 1 means good correlation with the RPC-LAP ion current and 2 good correlation with the spacecraft potential and 3 indicates no good correlation with any of the RPC-LAP parameters. The correlation is not good most of the time, so the flag is in practice only useful to find the time periods when the correlation is good.

How the data can be formatted and worked with

A suitable way of working with the data is to read it into a multi-dimensional array with dimensions corresponding to time, azimuth, elevation, mass channel and energy. The elevation steps for 3D data may also be part of the time series. This can be convenient when plotting an energy spectrogram, one can then see the repeating pattern of the elevation scan. We show an example in figure 2

where we have summed over all mass channels and azimuth angles, retaining time and energy, with elevation information being part of the time series.

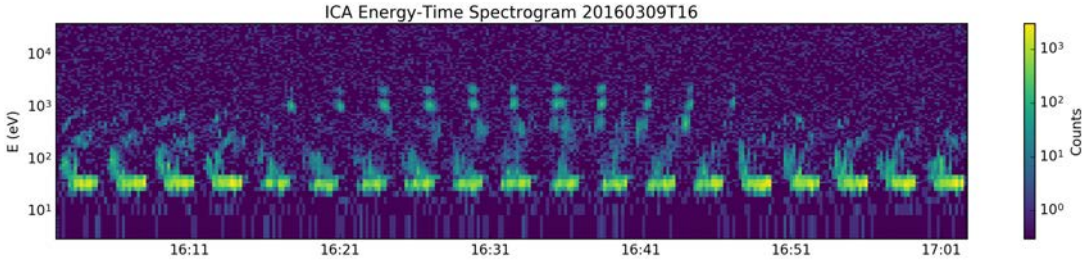

Figure 2 Energy spectrogram example from 2016-09-03. The elevation information is retained and seen as repeating patterns in the time series.

Another useful way of looking at the data is by summing over time and azimuth, retaining mass channel and energy information. One then obtains an "energy mass matrix" which can be used to determine the mass of the different observed ion populations.

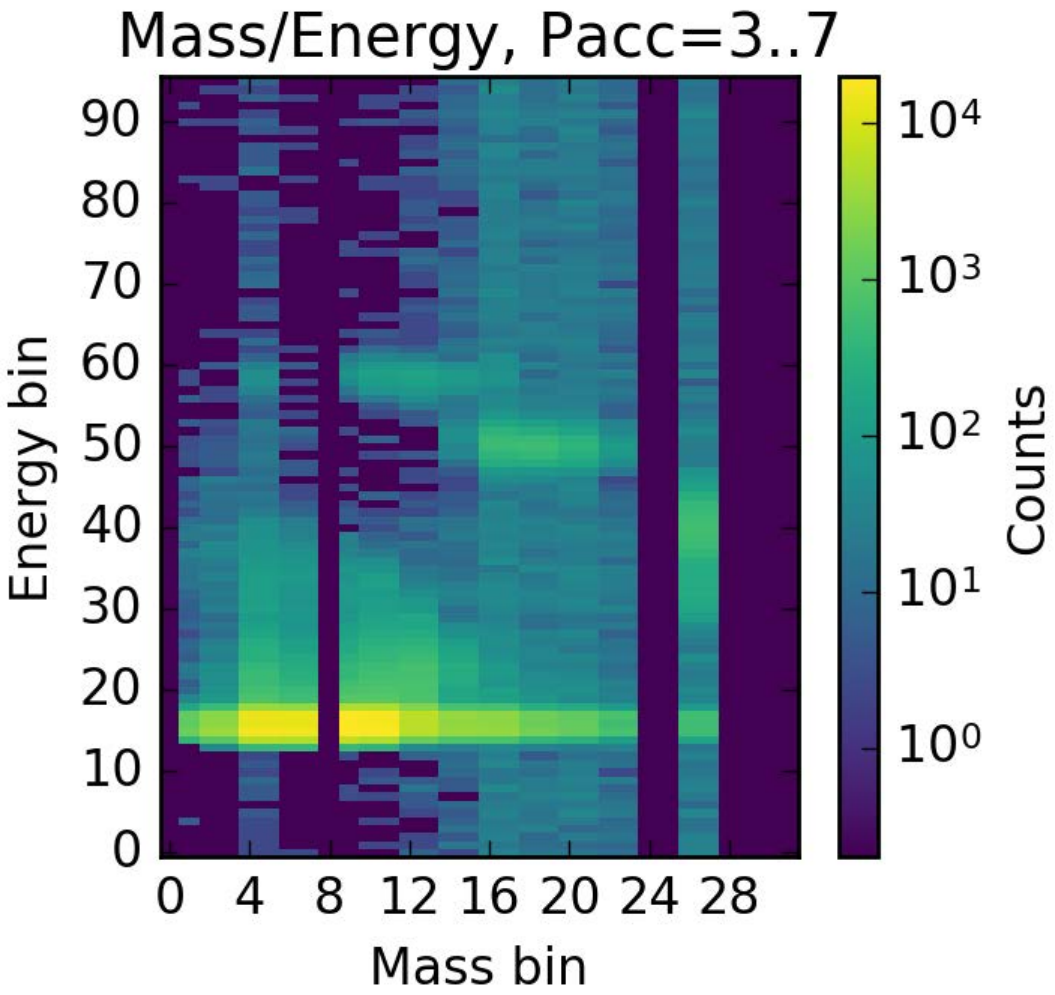

Figure 3 Energy - mass matrix for the one hour sample data shown in Fig. 2.

Mass separation is further discussed in section "Mass separation". Inspecting the mass matrix gives an indication whether there may be cross talk, i.e. a wide horizontal line extending from a strong signal across all mass channels at the same energy. This can be seen for energy bins around 15 in our example shown

in figure 3. One can here also see that RPC-ICA has several dead or nearly dead mass channels. This is mainly a problem for the detection of H^+.
A rough directional overview can be obtained by summing over energy and mass channels and then plot counts for each azimuth as function of time. If elevation information is retained as part of the time series then this can provide a first overview, but only for short time periods when the elevation information can be resolved.
Once the data analysis gets more advanced one will want to separate the ions into physical ion masses, possibly different energy ranges for the cometary ions and look at the full flow direction. This is further discussed in sections "Mass separation" and "Working with geometry data".

Calibrated data

Raw data (L2) is delivered to the archive. This may be the best data to use when looking for very weak signals or when the user wants to do some particular data processing before applying calibration factors. The team also delivers L3 data that is in the same form as the L2 data, but in units of differential flux [particles / cm^2/s/sr/eV]. The L4 data has been processed to remove cross talk and other artefacts and noise is treated in a consistent manner. This should in general be the preferred data for those who want to deal with the data in full detail. Finally there is one more calibrated data set, the mass separated data set. This is the easiest data set to use. Masses have been separated into the main physical mass ranges. Cross talk between masses has been removed as far as possible, and when there is doubt, the signal in the mass range with a weaker signal has been removed. For solar wind ions a manual selection of energy and mass channel ranges has been used. This is thus a conservative approach. Some weak but real signals may be missing in this data set, but it is otherwise the safest and easiest data to use.

How to go from L2 to L3

In order to calculate differential fluxes from the raw count data, the geometric factor of the instrument is needed. It is provided as files in the archive in the CALIB/GFACTOR directory, two files per software version, one for heavy ions and one for light ions. The GFACTOR files contain 8 different values for different post-accelerations (0 – 7).

In order to separate between light and heavy ions mass masks are supplied in directory CALIB/MASS_MASKS, likewise two per software version, one for heavy and one for light ions. The mass masks have the value 1 for energy – mass channel combinations corresponding to light / heavy ions. Dead and problematic (prone to pick up cross-talk) mass channels may be 0 in both masks. In particular mass channel 4 which is very prone to pick up cross-talk is set to zero in the heavy ion mass mask. There is also a range of high mass channels that for high energy does not correspond to any real particles. For the L3 data a count to flux conversion was performed for all data points, so for the user to reproduce the L3 data the data points that are zero in both masks must be changed to 1 in one of the masks. For the high energy, high mass channels part, this is closest to the light

ions, so this was used in the production of L3 data. Any other mass channels were set according to their nearest neighbours.
There are three different files for different post-acceleration ranges:

TABLE	SETTING
1	0- 1
2	2-4
3	5-7

Note that the expected response (G factor) and position on the detector plate (mass mask) behave in somewhat different ways when changing the post-acceleration reference value.

Before proceeding and applying the appropriate geometric factor a correction for the deadtime of the detector should be performed. It is a statistical correction, taking into account that the instrument needs some minimum time between two consecutive detections in order to detect both. This will only affect strong signals and does not have a major impact for most of the measurements. The deadtime for the detector Tdead is 2 μs, the acquisition time for each energy level t0 is 120.9 ms. If the total number of counts during the acquisition (for all sectors and mass channels) is N then the corrected counts C_{corr} is given from the measured counts C by the following formula:

$$C_{corr} = C * (1 + N * Tdead / t0)$$

Note that N should be the sum over all sectors and mass channels as only one valid detection anywhere in the system can be made at one time. For most cases this gives only a minor correction.

One should next format the data so that for each sector, elevation and time one can multiply the energy mass matrix with the mass mask. After this the geometric factor for current post acceleration and ion mass range can be used. The formula to go from counts to differential flux is

$$\text{Differential flux} = C_{corr} / (G * tau * E)$$

where G is for the appropriate mass range, tau in s and energy E in eV. For RPC-ICA, tau is 120.9 ms. The geometric factor is in units of cm^2 sr eV/eV, with the energy resolution being part of the geometric factor. The geometric factor for different software versions and post-acceleration levels are given in tables in the CALIB directory.

Mass separation

The best way to perform a mass separation is to plot a mass matrix for the time period of interest, or if necessary for several shorter subsets. We show below an example from 2016-03-12 between 15:00 and 16:00. Lighter ions are found at

higher mass channel numbers, heavier ions towards lower numbers. Ions with higher energy are also found at lower mass channel numbers, so that at high energy all masses are found in the upper corner of the mass matrix, and the mass separation is less reliable. During the Rosetta mission, the solar wind ions were almost always separated not only in mass, but also in energy. One therefore seldom actually need to know the precise expected position of H^+, He^{2+}, He^+ to separate them. Defining a box in the mass matrix, as we have indicated in figure 4, is the best way to pick out ions of a certain mass. This is how the solar wind ion data in the enhanced archive L4 PHYS-MASS data set has been produced. In figure 4 we also indicate the cross-talk produced by the intense proton fluxes. This is seen as a band covering all mass channels, also those corresponding to heavy ions. In the L4 PHYS-MASS data set cross talk has been suppressed by comparing the counts corresponding to heavy and light (1-4 amu) ions for each sector and energy step. Only the dominating ion mass range is retained, i.e. the one with most counts, the other one is put to zero. To suppress cross talk spreading to other sectors than just the one with the original signal, there is also a check on the sum over all sectors. If the sum over sectors of the minor mass population is smaller than one third of the sum of the dominating mass population, the minor population is put to zero. The PHYS-MASS data set is thus a conservative estimate, some real data may have been removed. In our example in figure 4 one may discern some signal between He^{2+} and He^+, this likely corresponds to the presence of multiply charged ions in the solar wind, such as O^{6+} and O^{7+}. This sometimes occur more clearly at energy levels corresponding to their mass per charge assuming they move with the same velocity as the other solar wind ions. These ions are not retained in the PHYS_MASS data set. The user needs to identify them from the full data set (L2, L3 or L4 CORR).

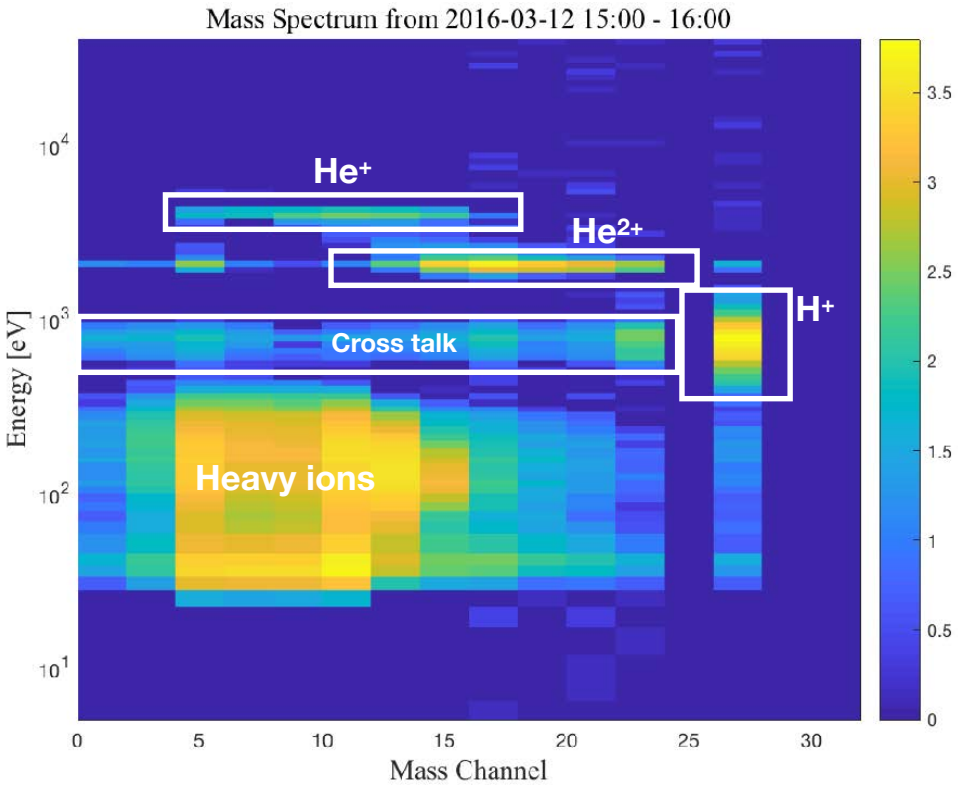

Figure 4 Mass matrix with sample ion selection boxes

The line dividing heavy ions from lighter ions can conveniently be obtained either from the mass masks provided in the CALIB directory or from the on-board mass lookup table for software version 9 also provided in the CALIB directory. Note that on-board tables for other software versions are not useful, they reflect what was actually on-board but are not fully correct. In figure 5 we show another mass matrix summed over 1 hour, with 3 lines from the mass lookup table corresponding to software version 9. The white line is the upper limit for heavy ions, column 6 of the lookup table, and two red lines showing the upper and lower limit of He^{2+}, i.e. columns 9 and 10 of the lookup table. The lookup table of software 9 attempts to maximize the information retained when on-board data binning using mass tables is used. Columns 1 and 2 always contain all valid mass channels (1 to 27). Columns 3 and 4 gives the lower half of mass channels corresponding to heavy ions, while columns 5 and 6 give the upper range. Column 6 thus gives the upper range to use for heavy ions. Columns7 to 12 give approximate upper and lower bounds for He^{+}, He^{2+} and H^{+} respectively. However, for low energies where H^{+} falls outside the detector plate, columns 11 and 12 correspond to mass channel 4 (starting from 0), a mass channel prone to pick up cross-talk.

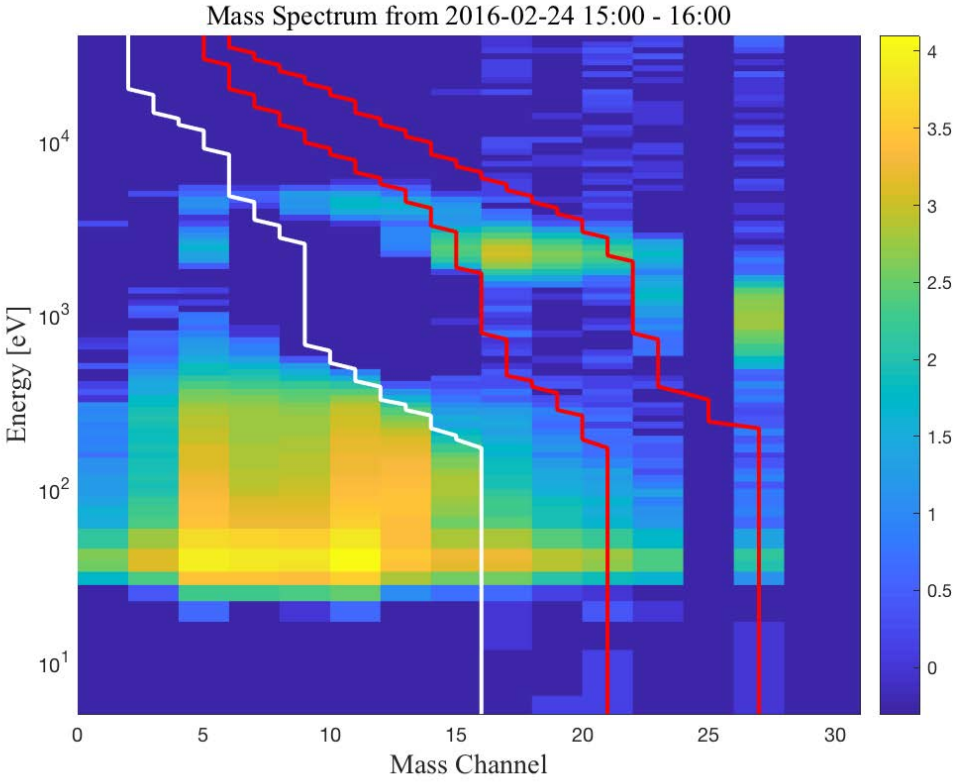

Figure 5 Mass matrix with mass lines from the mass lookup table of software version 9

Note that the sample mass matrices shown here were acquired in high angular resolution mode, so that mass channels were binned two and two on-board. Depending on how efficient the lossless compression was and on available telemetry, the data can be more binned according to the mode variable, see table 3. In the archive data such binned data, also that binned using on-board mass lookup tables, is expanded to 32 mass channels. Such data can thus be treated in the same way as higher resolution data but may not be suitable for all types of scientific investigations.

Handling noise

There is a somewhat varying degree of noise in the data. Noise levels are higher when the instrument is cold. The instrument was run in warm up mode for a while before data acquisition began, but still a period with higher noise is often seen for some time after startup.

To make lossless compression more efficient, noise was reduced on-board through a background subtraction. The value of this background subtraction is given by the variable Noise reduction in the archive data. Typically a value of 2 was used. The background subtraction was performed after binning, so the actual subtraction varies. The enhanced archive L4 CORR data attempts to correct for this to give better statistical properties.

The mass separated data in the L4 PHYS-MASS data set takes another approach, setting all data points which, after mass binning, has less than 2 counts to zero. This typically makes for clean data and is suitable to use when there is no need to analyse weak signals.

Another method employed on data from the RPC-ICA twin instrument IMA of ASPERA-3 on mars Express is to put all data points where all neighbours in the energy – mass matrix are zero to zero. This is done as part of the L4 CORR data treatment. This seems usually not needed for RPC-ICA L2 data, but may be useful. One may also subtract the median along energy or along mass channels as a real signal is most of the time limited in both energy and mass channel extent.

Data with no on-board subtraction look noisy but may be suitable when looking for weak signals. It is not suitable for calculation of moments unless some type of noise subtraction is performed.

The energy table

The energy table is determined by the software version of the data and found in the energy tables in the CALIB directory. The low energy level of RPC-ICA is not exactly known. The best current estimate is used in the archive data. Comparison with the Langmuir probe estimate of the spacecraft potential has narrowed down the uncertainty to a few eV (Odelstad et al., 2017).

The early energy tables, software version 2 and 3, were problematic as discussed in Nilsson et al. (2015a, 2015b), there was a significant offset between the actual voltage of the electrostatic analyzer and that used to calculate the energy tables. The result was that the lowest energy steps were not useful, sampling of low energies was coarse and energy and elevation tables at low energy were mismatched. It is in general better to use data with software version 4 or higher, introduced 30 October 2014. Calibrated data (L3, L4) corresponding to invalid energy levels are set to “missing constant” value in the PSA data set.

Energy scale and temperature

The energy scale also drifts when the instrument is cold, see Nilsson et al. (2017) for more details. They gave a simple correction for the temperature drift as: $E_{corrected} = E + (13.5 - T_{sensor}) * 0.7$ when $T_{sensor} < 13.5$ °C. For higher sensor temperature no correction is needed. The temperature is available in the housekeeping data (HK) in the PSA L2 archive. The sensor temperature is found in position 4 of the HK files. Details are given in the data label and EAICD. A flag in the data is set when the instrument temperature is low. The instrument temperature is lower just after start-up, but also a function of heliocentric distance, spacecraft orientation and use of a spacecraft controlled heater. The temperature was problematically low mainly in May 2015, after that the use of the spacecraft controlled heater was improved to avoid the worst temperature changes, in particular the lowest dips in instrument temperature.

A data set with temperature and spacecraft potential correction is delivered as part of the enhanced archive. The corrected energy scale is delivered as a separate file with the data, one energy scale per time stamp of data. The RPC-LAP spacecraft potential estimate is delivered as a separate file, with the data interpolated to the times of RPC_ICA measurements.

Energy stepping

The actual energy stepping of RPC-ICA is from high energy to low. In the archive data this order has been reversed as it is easier to work with the data if it goes from low to high.

To achieve high accuracy, the RPC-ICA instrument first steps a high voltage on the inner electrostatic analyzer plate while keeping the potential of the outer plate constant. At some voltage the situation is reversed, the voltage on the inner plate is fixed and the low voltage of the outer plate is stepped. A peculiarity in energy tables 4-6, 9 and 10 is that the first energy step after changing which plate we step is lower than originally planned. For these energy tables the data has been re-ordered so that the energy table is monotonic.
We show an example of the relevant part from software version 9 in table 4.

Table 4 Sample part of energy table of software version 9

Index (starting at 0 and low energy)	13	14	15	16	17	18	19	20	21
Energy on board [eV]	61	66	71	77	68	89	99	109	119
Energy in archive data [eV]	61	66	68	71	77	89	99	109	119

In the index column we show data where the outer plate is stepped with light grey shade, and light blue shade for data when the inner plate is stepped. This ordering shouldn't matter to the user except for the fact that we sometimes see a peculiar behaviour of the energy step marked with red shading. We show an example in section "Strange signals in the data". The signal in energy step 17 is sometimes higher, sometimes much lower than surrounding data. Energy step 16 is sometimes also affected, but typically less. The clearest case is an artificial looking line with very low signal for energy step 17 which sometimes occur, mainly from May 2016 and onward. The index of the problematic energy step is given in table 5 for the relevant software versions (those not listed do not have this problem). Note that in the on-board ordering, it is the first energy step when

the inner plate is stepped that is sometimes problematic (timewise, energy steps from high to low energy).

There is another step-like change that does not directly relate to the energy spectra, but which can be seen in them. From energy step 19 (for software versions 4,5,6, 9 and 10) there is a step like change in the elevation coverage. Below that level, due to limited resolution, there are actually only 8 different usable elevation values. For these low energies each elevation value is repeated twice, and for the very lowest energies many of these elevation steps (at low and high extremes) do not correspond to useful angles of deflection and does not let any particles through. An abrupt change can often be seen in energy spectrograms at energy level 19.

Table 5 Index where stepping changes between inner and outer plate

Software version	4	5	6	9	10
Change of step (starting from 0 and at low energy)	17	18	18	17	17

For software versions 7 and 8 only the outer plate is stepped. The original 96 energy step table has been given a saw-tooth form with an 8 or 32 energy step pattern repeated. In the archive data the repeated patterns have been split into data with 1s or 4s resolution and 8 or 32 energy steps.

Working with geometry data

Coordinate systems

RPC-ICA has a Cartesian instrument coordinate system, as illustrated in figure 6. The most natural description of the field of view is given by the angles corresponding to the sector and the elevation, as also illustrated in figure 6.

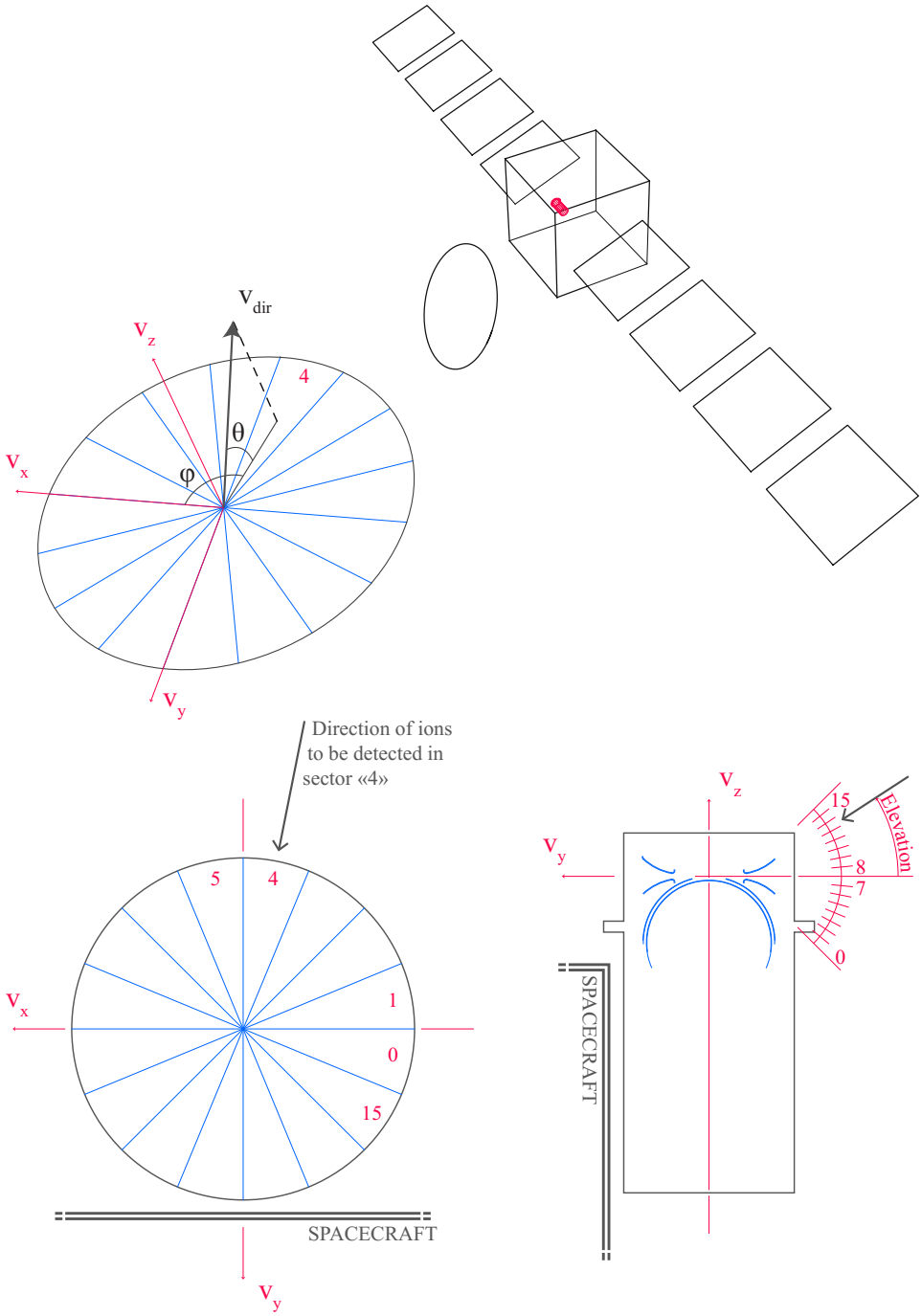

Figure 6 Illustration of the azimuth and elevation angles (top left) and the RPC-ICA instrument coordinate system. The location of RPC_ICA on the spacecraft is also shown in the top right of the figure. Note that the sector numbering here indicates the view direction of the sector of the sector, not the physical location of the sector which is the opposite (and which is used in for example the ICA_CAL.PDF document delivered with the archive data).

The azimuth angle is defined from the sector number as given in table 6.

Table 6 Azimuth angles for sector index

Index	0	1	2	3	4	5	6	7	8	9	10	11	12	13	14	15
Angle	168.75	191.25	213.75	236.25	258.75	281.25	303.75	326.25	348.75	11.25	33.75	56.25	78.75	101.25	123.75	146.25

This can simply be calculated as

Azimuth = (sector_index+7.5) 2 π /16 mod(2 π)

Which gives the angle in radians for each sector index.
The elevation angle corresponding to a particular elevation index and energy for a given software version is given by the elevation tables in the CALIB directory. We show as an example the elevation angles of software version 9 in figure 7. Note that the elevation angle is the angle from the symmetry plane, i.e. it is not the polar angle of a typical polar coordinate system.

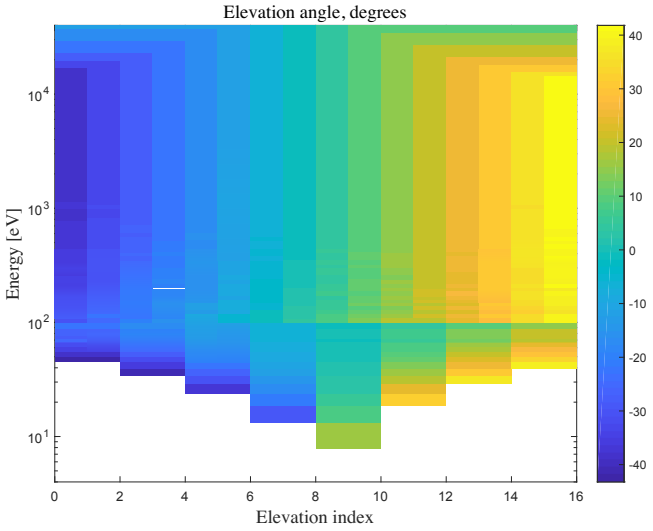

Figure 7 Elevation angles as function of elevation and energy indices.

Given the azimuth and elevation angles unit vectors of the look direction can be calculated in the ICA instrument reference frame as
v_x = cos(elev) cos(azim)
v_y = cos(elev) sin(azim)
v_z = sin(elev)
where the ICA instrument frame is defined and illustrated in Nilsson et al. (2007). X of the instrument frame is the same as the spacecraft reference frame, while instrument Y is along spacecraft -Z and instrument Y is along spacecraft Y. Thus one get a more natural coordinate system to take spacecraft attitude into account:
v_x = cos(elev) cos(azim)

v_y = sin(elev)
v_z = -cos(elev) sin(azim)

If spice kernels are available to the user, the spacecraft reference frame can easily be turned into any suitable coordinate system, often CSEQ (Comet Sun Equatorial) is used. In the PSA L2 archive GEOM files are provided giving the position and spacecraft attitude in the local target coordinate system, CSEQ for comet 67P. The attitude is found as 3 unit vectors (spacecraft X, Y, Z) with each 3 components (CSEQ X, Y, Z), in column 9 of the GEOM files. See data label or EAICD for more details. The spacecraft unit vectors can then be used to transform the data into the target frame, i.e. CSEQ for comet 67P.

Working with the field of view

The field-of-view of RPC-ICA is not complete. Apart from only covering elevations angles up to about 40°, part of the field of view is blocked by the spacecraft. RPC-ICA typically had a free field-of-view towards the sun and the comet. It is believed that much of the time the limited field-of-view was not a major problem. There are however clear cases when the spacecraft blocking of certain direction strongly influences the signal seen in the data.

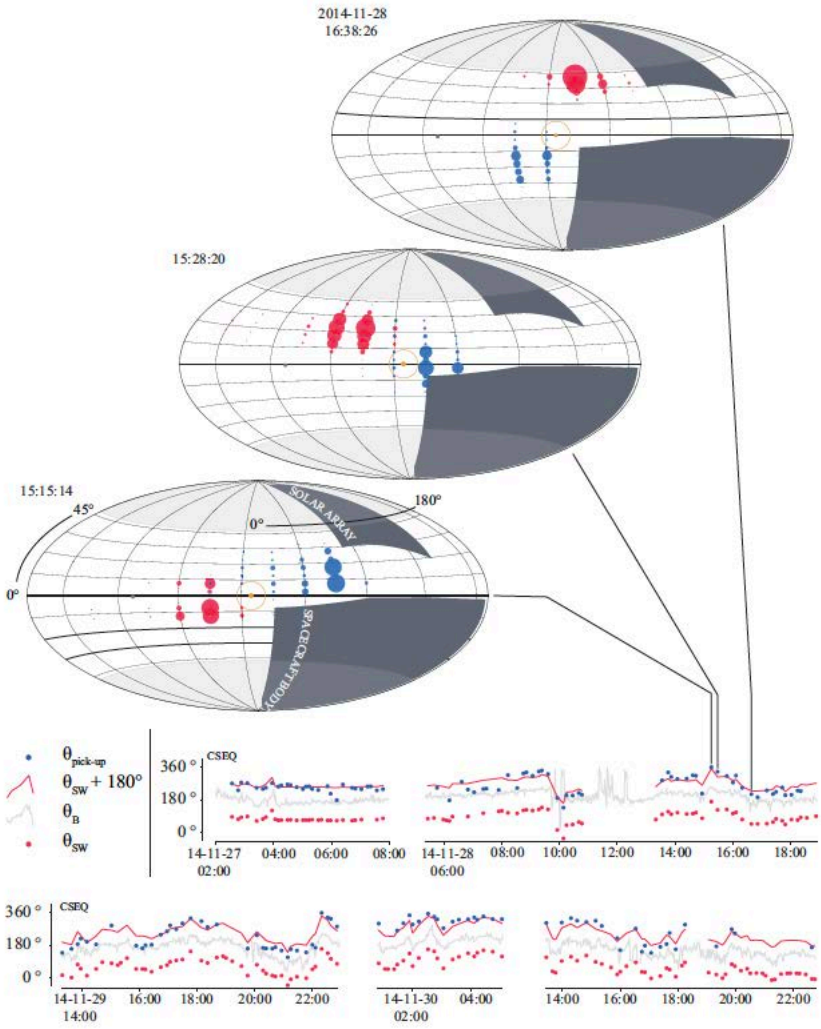

Figure 8 The RPC-ICA field-of-view with sample signal shown in red (protons) and blue (heavy ions) from Behar et al. (2016)

Figure 8 shows the field of view of RPC-ICA as function of the azimuth angle (horizontal) and elevation angle. The spacecraft body and solar panel obstructions are indicated with dark grey, unreached elevation angles with light grey shading. The Sun in a typical position is shown with a yellow dot, and the comet as a black dot. Observed signals are shown as dots varying in size according to the strength of the signal. Red indicates protons and blue heavy ions. This is an example on how one can inspect whether the blocked field of view affects the observations of some particular identified signal. If the signal is close to the limit of being in the free field of view one must be careful. Abrupt changes in the signal may then be related to the ion flow moving in and out of the free field of view. Most, if not all, abrupt changes in solar wind and cometary ion signals appear to be related to the field-of-view.

The incomplete field of view can to some extent be remedied by comparison with the ion data from the RPC-IES instrument. The field of view of the two instruments partially overlap but also partially complement each other. The RPC-IES field of view from the RPC-ICA view point is shown in Fig. 9.

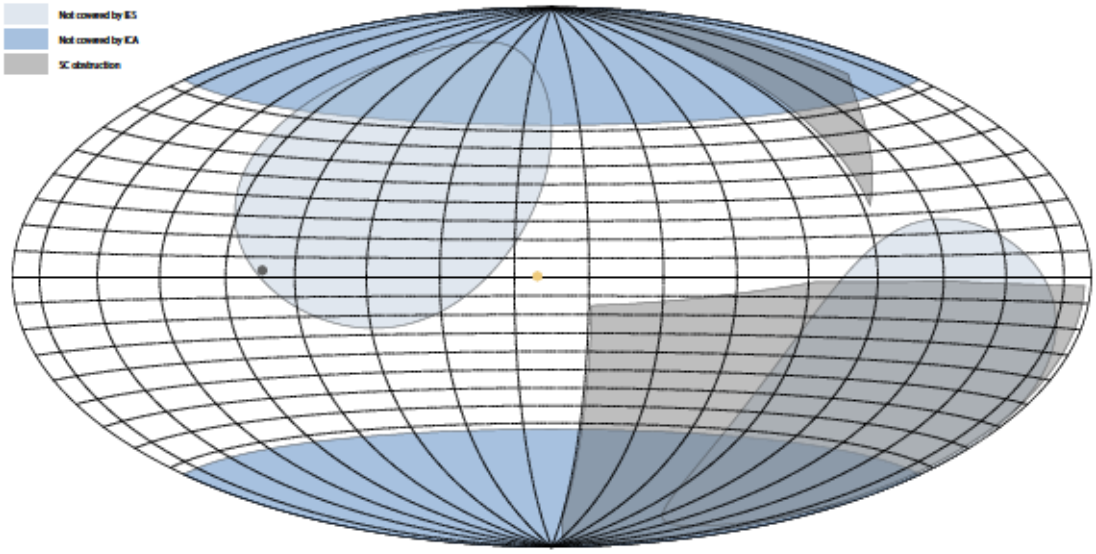

Figure 9 The IES field of view shown from the ICA point of view. Medium blue shows directions not covered by ICA. Grey shows regions blocked by the spacecraft. Blue-grey shading show the regions not covered by IES.

The combined instruments cover a significantly larger part of angular space. This is often seen in solar wind ion data, where the proton and alpha particle signals can often be seen to weaken in the data from one instrument only to increase in the data from the other instrument.

Strange signals in the data

We here list a few typical examples of data that are considered suspicious by the instrument team.

An example from 27 May 2016 displaying several suspicious behaviours at the same time is shown in figure 10.

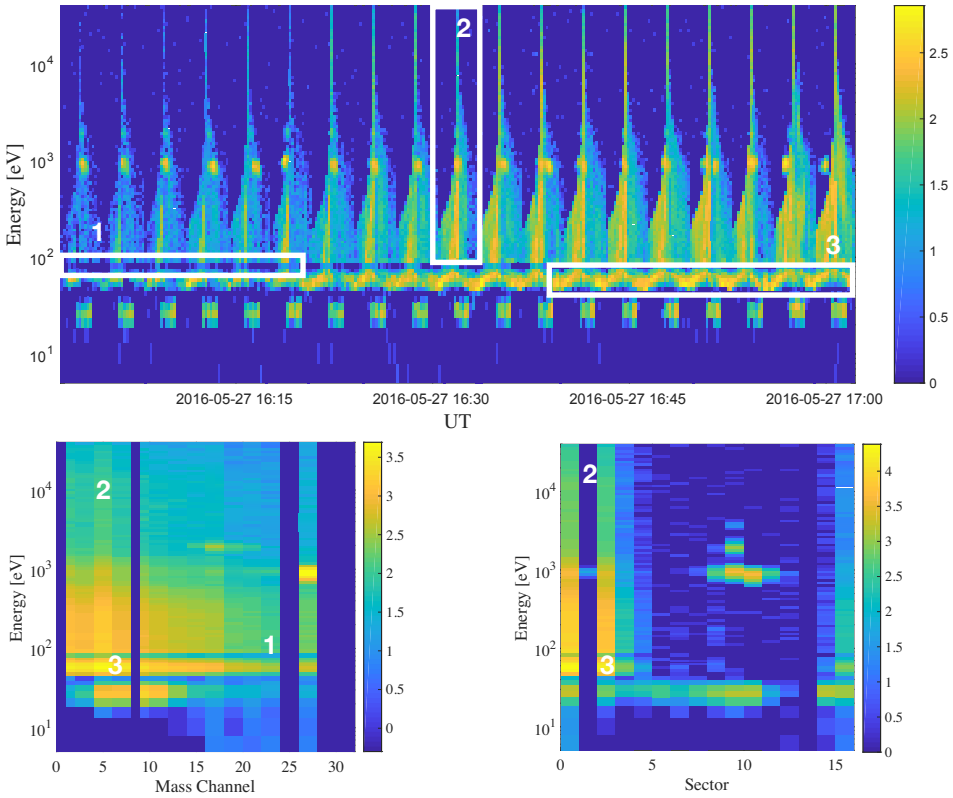

Figure 10 Example from 2016-05-27 showing 3 different types of data of uncertain nature

The upper panel of figure 10 shows an energy time spectrogram, summed over all sectors and mass channels. The lower left panel shows a mass matrix, mass channel on the X axis, energy on the Y axis and summed counts on the colour scale. The lower right panel shows a plot with sector number on the X axis and energy on the Y axis.
The feature number 1 of figure 10 is the same feature discussed in section "Energy table". It is a local minimum at a more or less constant energy step, the straightest line seen visually corresponds to energy step 17. It can here be considered to be part of feature 2, a signal extending over almost all energy steps where the inner plate of the electrostatic entrance deflection is stepped. Feature 2 is seen on sectors 0, 2 and 15. These are sectors prone to pick up cross-talk and show enhanced noise. The mass channel distribution is rather wide, also at high energy. The strongest signal is seen in mass channel 4 which is prone to pick up cross-talk, but this likely just reflects that we have a broad signal. The signal over a large energy range is suspicious, as the IES instrument did not detect anything similar, even when the signal was in the IES field of view. The signal has a peculiar pattern with elevation (elevation is part of the time series in figure 10).

Feature 3 finally is a signal at relatively low energy, but well above the persistent low energy signal. It shows some modulation of energy with elevation. In the example in figure 10 the mass response is rather broad and shifted towards lower mass channels as compared to the regular signal. It can be a real signal corresponding to heavier ions than the usual water group ions. The sector

distribution is the same as for the suspicious high energy signal. These signals were typically observed towards the end of the mission when passing very close to the nucleus. This speaks against the high energy particles being real ions. There is a similarity to the high energy signal seen in RPC-IES electron data which was interpreted as negatively charged nano-dust (Burch et al., 2015). If there really was positively charged nano-dust one would expect that to be seen in RPC-IES as well. Therefore it is currently believed that this signal is an instrument response to the gas and ion environment at close distance, but cannot be interpreted as high energy ions. Feature 3 was not observed in RPC-IES data either, but it could be due to poorer energy resolution of RPC-IES at low energy.

Another feature sometimes seen in the data is shown in Figure 11, a population below the main low energy population, also seen at energies thought to correspond to non-valid energies (less than zero).

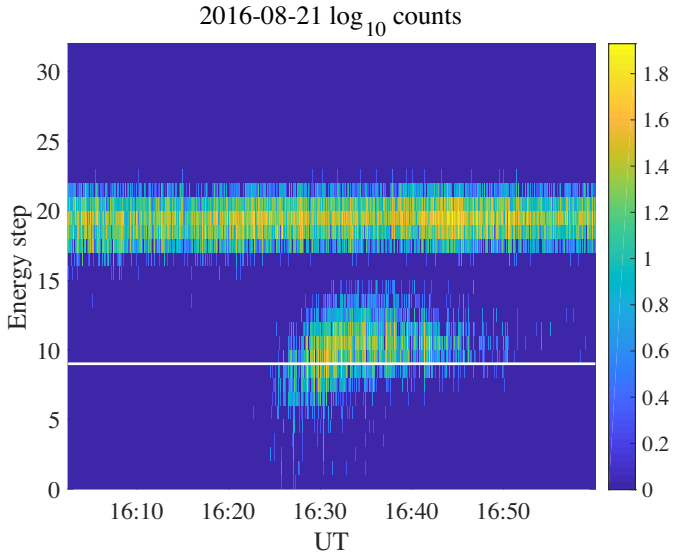

Figure 11 Low energy population. The white line indicates the border of valid energy steps.

In figure 11 the Y axis shows energy step. A white line indicates the border of valid energy steps. It is not known what causes this signal. The mass response is typically strong at high mass channels, thus corresponding to light ions. The sector distribution varies.

Flagging strange signals in the data

We currently flag two types of extra-ordinary data, a signal seen over a broad energy range (feature 2 of our first example) and a low energy signal in our second example. The flag values and features are summarised in table 7. Data are flagged over 1 hour intervals, if the feature occurs within a 1 hour interval, all data for that interval is marked with the flag.

Table 7 Extra ordinary data flags

Flag number	Feature
0	No known problem
1	Broad high energy signal
2	Very low energy signal

Caveats

Data affected by specific commands

Certain commands affect the data in a way that is not seen in the data structure used in the telemetry or the archive. This concerns commands where the energy or elevation stepping was set to a fixed value. Periods affected by such commands are shown below.

Entrance deflection set to fixed

When entrance deflection was set to fixed the elevation scanning was not performed. This is not reflected in the archive data, one need to look at the commands sent to the spacecraft. The table below lists the times when the entrance deflection was set to fixed. The next off time is also listed as this is for how long the entrance value was fixed. On a number of occasions the actual value of the fixed entrance deflection was changed before the instrument was turned off. In the third column the entrance deflection value is given. The value found to be closest to 0 and thus suitable to use for fixed elevations was an index value of 3.

Start time	Next off command	Value
'30-Sep-2014 20:18:22'	'30-Sep-2014 21:50:23'	4095
'30-Sep-2014 20:33:22'	'30-Sep-2014 21:50:23'	0
'30-Sep-2014 20:48:22'	'30-Sep-2014 21:50:23'	1
'30-Sep-2014 21:03:22'	'30-Sep-2014 21:50:23'	2
'15-Oct-2014 17:18:22'	'15-Oct-2014 18:50:23'	1
'15-Oct-2014 17:38:22'	'15-Oct-2014 18:50:23'	2
'15-Oct-2014 18:08:22'	'15-Oct-2014 18:50:23'	3
'22-Oct-2014 18:38:22'	'22-Oct-2014 21:20:23'	4095
'22-Oct-2014 18:58:22'	'22-Oct-2014 21:20:23'	1
'22-Oct-2014 19:38:22'	'22-Oct-2014 21:20:23'	2
'08-Dec-2014 21:00:22'	'08-Dec-2014 23:00:23'	2
'17-Dec-2014 09:09:22'	'17-Dec-2014 11:00:23'	2
'15-Jan-2015 12:00:22'	'15-Jan-2015 16:00:23'	2
'13-Aug-2015 07:41:22'	'13-Aug-2015 16:15:23'	3

Energy level set to fixed

This was only used once during the mission, and was reported in Stenberg Wieser et al. (2017). By keeping both deflection and energy level constant a value is obtained every 125 ms. The command to set the energy level to fixed was issued 13 August 2015 at 07:42:22 and the instrument was turned off at 16:15 the same day.

Low instrument temperature periods

The instrument temperature was dependent on the heliocentric distance, the spacecraft attitude and a spacecraft controlled heater. When the instrument became too cold, noise levels increased and the energy scale started to drift. Data

when there is a problematically low instrument temperature is flagged in the data. The worst period in terms of temperature was May 2015, a period also suffering other problems (see below).

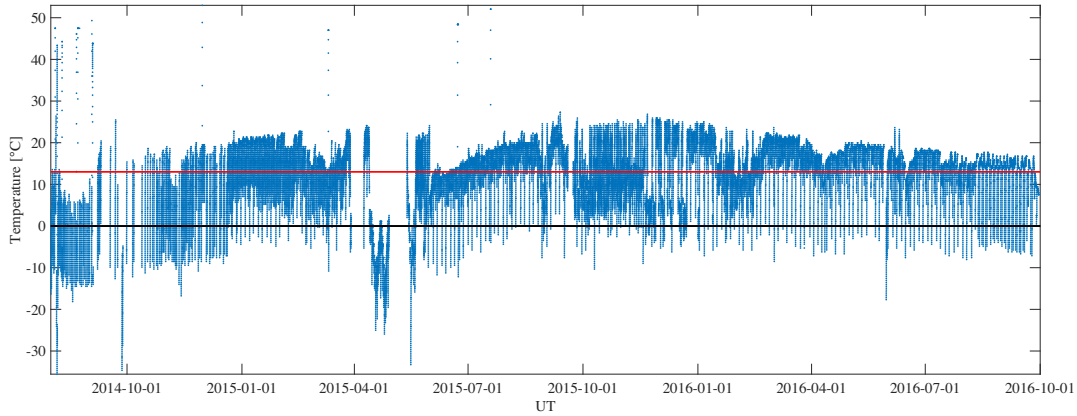

Figure 12 RPC-ICA sensor temperature throughout the mission. Red and black lines correspond to thresholds for increasing problems with energy scale drift.

In Figure 12 we show the RPC-ICA sensor temperature throughout the main mission. As mentioned earlier, the RPC-ICA energy scale is stable at temperatures above 13 °C, indicated with a red horizontal line in figure 12. Below 0 °C the drift is more severe, indicated with a black line. The drift is usually a few eV, but below 0 °C the drift exceeds 10 eV and may reach up to a few ten eV. It is thus a problem for the interpretation of low energy ion data. Ions at solar wind energies are never significantly affected. The large spread seen in figure 12 mainly reflects that the instrument was cold for a while after turn on.

Invalid software version and mode combinations

During May 2015 there was reason to believe that the RPC-ICA instrument had a problem with its high voltages. In the end it turned out to be a combination of low instrument temperatures and undetected corrupt data that caused the observed signatures in the data. While this was being investigated, RPC-ICA was run using software version 7, which use only low voltages on the electrostatic analyser and at the entrance deflection plates. There was not enough telemetry to download data without elevation binning. Therefore the resulting data has 4 s resolution within each nominal energy scan, but several energy scans were binned together on-board. That this data is problematic can often be seen by visual inspection, but it is not seen in the data structure as all data in the archive has been expanded to full resolution. A quality flag is used to indicate this type of data.

Data at small cometocentric distances at the end of the mission

As discussed in section “Strange signals in the data” there are a number of features seen in the data that are not fully understood. These were observed towards the end of the mission and typically at small cometocentric distances. An attempt has been made to identify such data and set a quality flag to a non-zero value for such time periods. We also refer the user to the examples shown in “Strange signals in the data” as the quality flag algorithms may not catch all cases.

L5 Data Moments

The ion distribution functions observed in the vicinity of comet 67P were seldom Maxwellian. Furthermore the instrument field-of-view is not complete. Despite this, ion moments can still be convenient to work with. The bulk velocity is still a good indication of how the ions are moving, and the density estimate is also useful. One must however be aware of the significant limitations of the RPC-ICA moment data. Some things to consider are:

The instrument field-of-view is incomplete. Low fluxes in the data may not correspond to low fluxes in reality, and in particular sudden changes of the flux often corresponds to a change of flow direction rather than an actual change of the flux. For the solar wind, sudden drops in solar wind ion fluxes are essentially always due to a changing flow direction, bringing the main signal outside the instrument field of view. This can usually be seen through a corresponding change in the flow direction of pick up ions (here defined as more energetic cometary ions having been accelerated by the solar wind electric field) and by a change in the direction of the magnetic field. The team have tried to see if a flag that warns when the maximum signal is at the edge of the field of view could be useful, but the predictive power of low densities was rather poor for the solar wind. For cometary ions the peak of the measured signal was very seldom at the edge of the field of view. One way of seeing if the H^+ signal was out of the field of view while the He^{2+} signal was in the field of view is to set a density ration threshold for the two ion species. Setting the limit of n_{H^+} to $n_{He^{2+}}$ to 1 or 0.1 identifies a large amount of the low H^+ density periods without setting a fixed limit to the low H^+ density.

For cometary ions, another additional problem is that there are several cometary ion populations, see for example Bercic et al. (2018). In the data delivered to PSA we have taken this into account in an approximate manner by dividing the cometary ion data set into two different energy ranges, below and above 60 eV. It may be possible to find a more precise division, but using 60 eV divides the data into a cometary ion population which almost always moves radially away from the nucleus in the Y_{CSEQ}-Z_{CSEQ} frame and another higher energy population which seems to be more affected by the solar wind electric field direction, as in the paper by Bercic et al. (2018).
The cometary ion distribution functions typically fall off rather fast with energy, meaning that the speed of the higher energy population will be quite strongly affected by the choice of the energy for splitting the two populations.

The precise position of the dividing line will not strongly affect the moments of the low energy population. For the higher level population it will somewhat affect the density and bulk velocity estimate. By not setting the limit too low, the velocity (direction) of the high energy population should not be unduly affected by the lower energy population. We discuss the two populations more later when we show some sample data.

Moment data delivered to PSA

The moment data delivered to PSA is based on the L4 PHYS-MASS data set. This means that we deliver moments for H^+, He^{2+}, He^+ and for heavier ions assuming the mass of H_2O^+. There may be more in the data, which the user will have to pick out from L3 or L4CORR data. Some artefacts in the data has also been removed in an ad hoc fashion. Still some problems remain in the data, as we will discuss later.

Data with too low angular resolution has been removed. We are only using data with instrument modes 8-12, 16-20 and 24-28. This corresponds to data with angular resolution 45° or better in both azimuth and elevation.
Data from software versions 7 and 8, corresponding to high time resolution 2-dimensional data, has not been used for moment calculations.

All data points where the data value is less than the L4 CORR uncertainty estimate has been put to zero. All data with less than 2 counts, after summing into physical mass bins, has also been put to zero.

Sectors 0 and 15 which are for certain parts of the mission very noisy, has been put to zero if the data was not more than 4 times the L4 CORR uncertainty estimate.

Finally, in order to remove some cross-talk related problems in the early data, sectors 0 to 4 has all been put to zero for the solar wind species for times before 2014-10-01. For times later than 2016-04-01, sector 0 has been put to zero for solar wind ions.

For the cometary ions, an ion mass of 18 amu (water) has been assumed. This is likely close to true during most of the mission.

If there are no counts detected corresponding to some mass, the density is calculated as zero. The corresponding velocity is given a “missing constant” value.

Solar wind moment data

Solar wind data requires some special consideration. The undisturbed solar wind is a narrow beam, something which RPC-ICA is not particularly well suited to measure. This is because the RPC-ICA field-of-view is obscured by the permanent magnets of the momentum filter at the boundary between azimuthal sectors. The fraction of a narrow beam seen may thus vary also when the solar wind is fully inside the nominal field of view. A mass-loaded solar wind mostly has a broader angular extent than the undisturbed solar wind, so this is less of a problem during most of the Rosetta mission, but may still matter. The solar wind beam may also be partly or fully outside the field of view of the instrument as mentioned above. The net result is that individual measurements of solar wind ion density is quite scattered and may not be very reliable. The velocity is much better determined. The best solar wind data set from Rosetta is obtained if solar wind moments from RPC-IES and RPC-ICA are combined, in particular as the two instruments total angular coverage is much better than that of any of the two

individual instruments. Currently there are no moment calculations based on data from both instruments, but a merged moment data set can rather easily be constructed. By interpolating the data from the two instruments to some common time and choosing the data from the instrument indicating the highest density for each time a smoother and more reliable data set is obtained.

Comparison with OMNI data

An advantage of the solar wind is that a cross-comparison with OMNI solar wind data can be done. In figure 14 we show a histogram of the ICA derived proton densities (blue bars) and the OMNI proton densities scaled to the position of Rosetta assuming a $1/R^2$ dependence (red). This could give the impression that the ICA densities are about an order of magnitude too low. This may indeed be true at times, but an inspection of how the ratio of the two densities evolves with time provides a different picture.

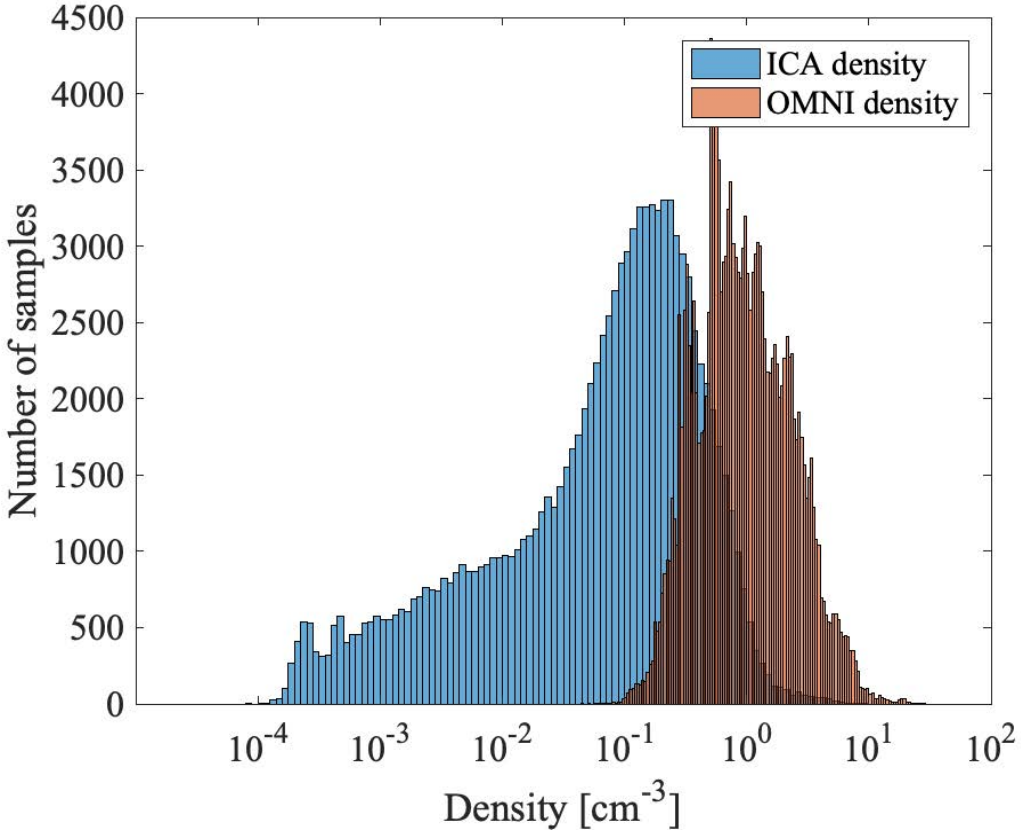

Figure 13 Histogram of the proton density from ICA (blue bars) and from the OMNI data set scaled to the Rosetta distance (red bars).

In Figure 15 we show the ratio of the proton density determined from RPC-ICA to the OMNI density, time shifted to Rosetta, as a colour coded histogram for each day (to make the plot readable). The upper limit is close to a ratio of one with

rather large scatter. The scatter around 1 is not surprising, as the time shift is far from perfect. If we had made a line or dot plot, the RPC-ICA data would fill up most time intervals down to the lower border of the plot. We therefore believe that the calibration is good, but individual values still carry a very large uncertainty.

We do not show velocity here, but in general the velocity estimate is more reliable than the density estimate. The velocity estimate may still suffer from the restricted field of view. There is a lower occurrence of high solar wind velocities in the RPC-ICA data set as compared to the OMNI data set, in particular above 600 km/s. The RPC-ICA distribution of H^+ and He^{2+} velocities look quite similar, tentatively indicating that the lower occurrence of really high velocities is not an effect of the dead mass channels affecting mainly H^+.

Comparison between protons and alpha particles

Another aspect to check with the data is the ratio of alpha particles to protons in the solar wind. This may change in the coma due to a higher charge exchange rate for protons than alpha particles, but should still be quite similar to the solar wind for much of the mission. The scatter in this ratio is rather large, the median alpha to proton number density ratio is 8 %. We show a colour coded daily occurrence rate of the ratio in Figure 16.

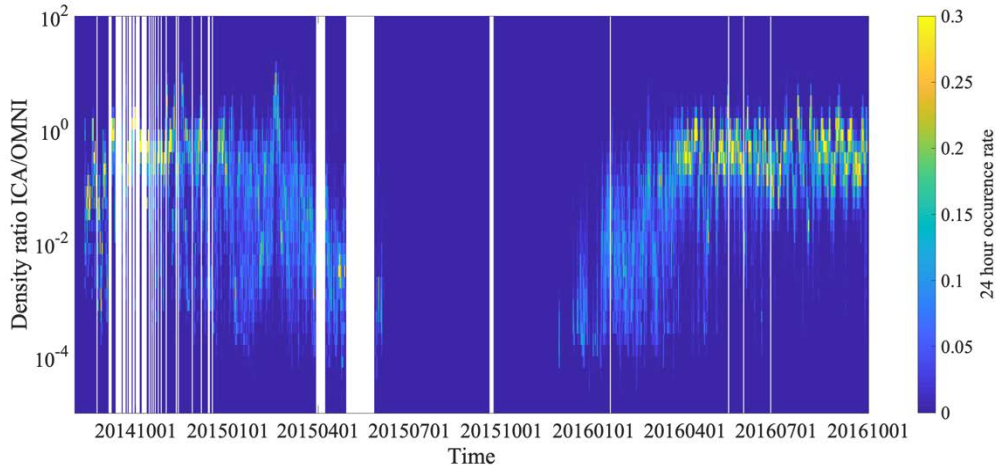

Figure 14 Colour coded daily histograms of the ratio between ICA and OMNI proton densities.

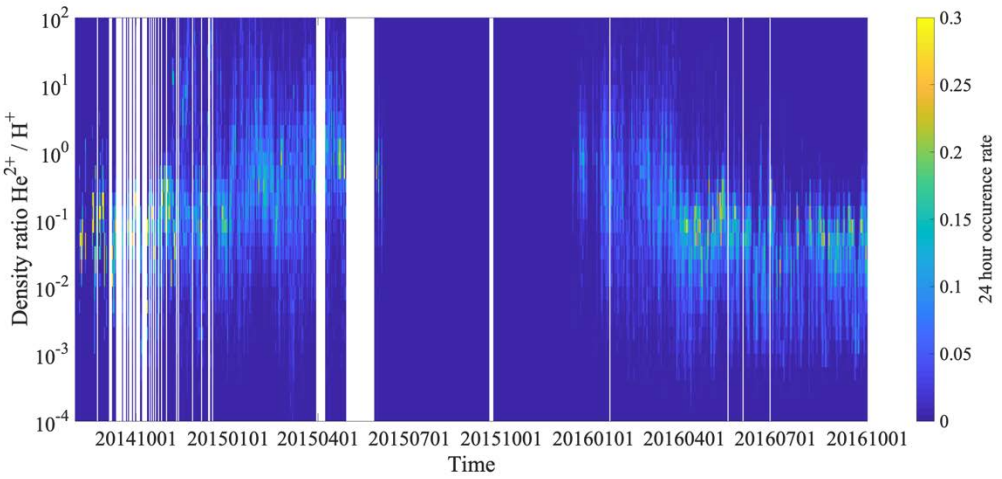

Figure 15 Colour coded daily histograms of the ratio of He^{2+} to H^+.

The He^{2+} to H^+ ratio increases around the solar wind ion cavity, when the H^+ density drops significantly compared to the OMNI derived densities. This is probably consistent with effects of charge exchange being more effective for H^+ (Simon Wedlund et al., A&A, 2019).

We have also investigated the He^{2+} to H^+ speed ratio. It turns out that the speed of He^{2+} is typically somewhat larger than for H^+. We have investigated if this can be an instrument artefact, but this currently seems unlikely. The energy scale is quite well known at the lower border, through comparison with the spacecraft potential (Odelstad et al., 2017). The energy at H^+ is well validated through comparison with OMNI and RPC-IES data. It is therefore not very likely that something happens to the energy scale between the H^+ and He^{2+} energies. Furthermore the mean speed of He^{2+} and He^+ are very similar. In Fig. 17 we plot the speed of He^{2+} as function of the speed of H^+, with the marker size a function of He^{2+} density and the colour a function of the H^+ density, for both species only for densities above 0.01 cm^{-3}.

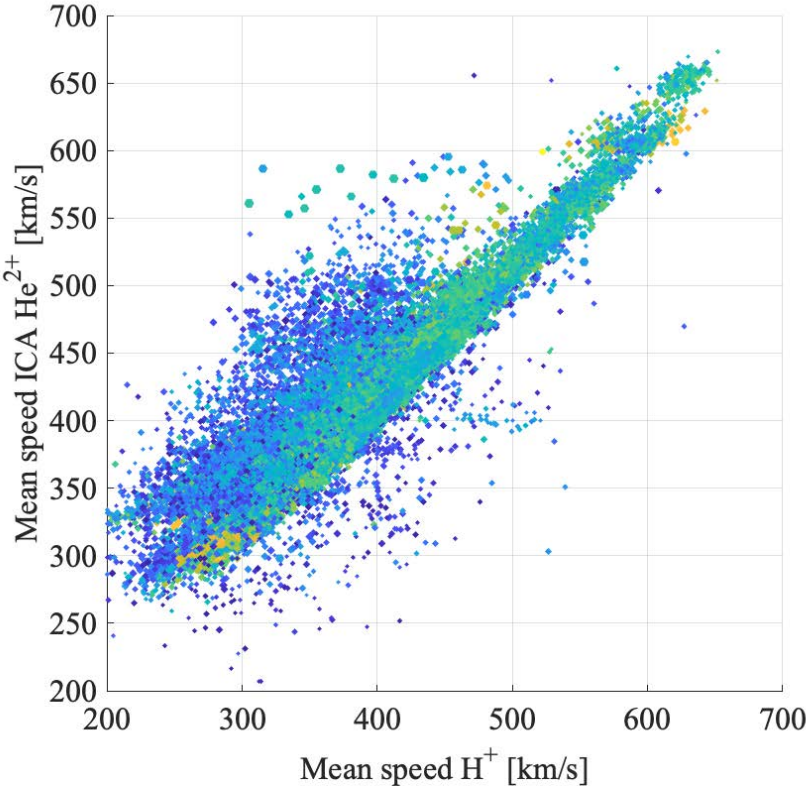

Figure 16 Comparison of the bulk speed of H^+ and He^{2+}, with size of marker a fucntion of He^{2+} density and the colour a function of the H^+ density.

The speeds essentially follow a linear trend, with He^{2+} velocities having a spread down to the speed of H^+, the difference being some 10%. There may be a physical explanation for the higher He^{2+} speed: The force per mass acting on the He^{2+} will typically be about half that acting on the H^+ due to the mass per charge ratio. This is seen in less deflection of the He^{2+}, but would also be the case for a force along the motion of the particle and thus cause less deceleration in the interaction with the coma. The good similarity between the H^+ speed and the OMNI data means that there can only have been very limited deceleration of H^+ during most of the observations, but of the order of 10% may still be feasible.

Cometary ion moment data

The cometary ion moment data delivered to PSA has been divided into two energy ranges, below and above 60 eV. The density of the low energy population is currently a significant underestimate of the real plasma density, which can be obtained using the LAP and MIP instruments. There are several possible explanations for this, where an erroneous geometric factor at low energy is one possible explanation. Other explanations which may have significant impact, if the plasma is a narrow beam in energy and angle, is a non-dense coverage in both elevation angle and energy at low energies. For now the ICA densities at low energy cannot be considered to be an estimate of the plasma density, though the covariation with the LAP and MIP density estimates is sometimes good. When a significantly negative spacecraft potential brings the ion energy up the ICA and LAP / MIP density estimates may become more similar. We show an example from 20150705 in Figure 18, where red circles show Lap data and black triangles

ICA data. The upper panel shows density estimates and the lower shows the negative of the LAP spacecraft potential and the $\log_{10}$ of the ICA density times an arbitrary factor to make the numbers similar. The day started with a significantly negative spacecraft potential and a decent similarity between the density estimates, where the somewhat lower ICA values can likely be explained by the limited field of view. After 9 UT the spacecraft potential becomes closer to 0, and both density estimates drop. The ICA density drops much more than the LAP density estimate, and becomes more than an order of magnitude lower. If we instead look at the lower panel (spacecraft potential) we see that we still have a correlation between the two data sets. In addition there are a number of density estimates from ICA which are 4-5 orders of magnitude below the other estimates. This indicates that the main plasma component in these cases is outside the ICA field of view or energy sampling space. For the data delivered to PSA, it seems that the ICA low energy density is typically some 2 orders of magnitude below the LAP and MIP estimates.

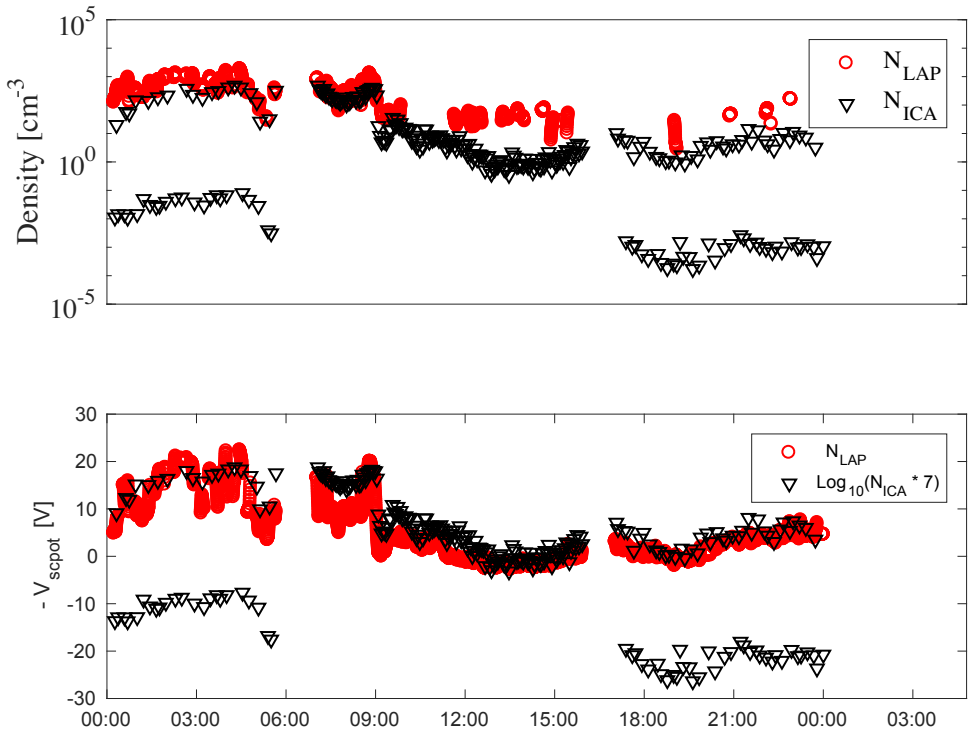

Figure 17 ICA (black triangles) and LAP (red circles) density estimates (upper panel) and negative of spacecraft potential (LAP) compared to the log10 of the ICA density estimate (lower panel).

Working with moment data

We start a discussion on working with moment data by showing moments integrated over 24 h in Fig. 19.

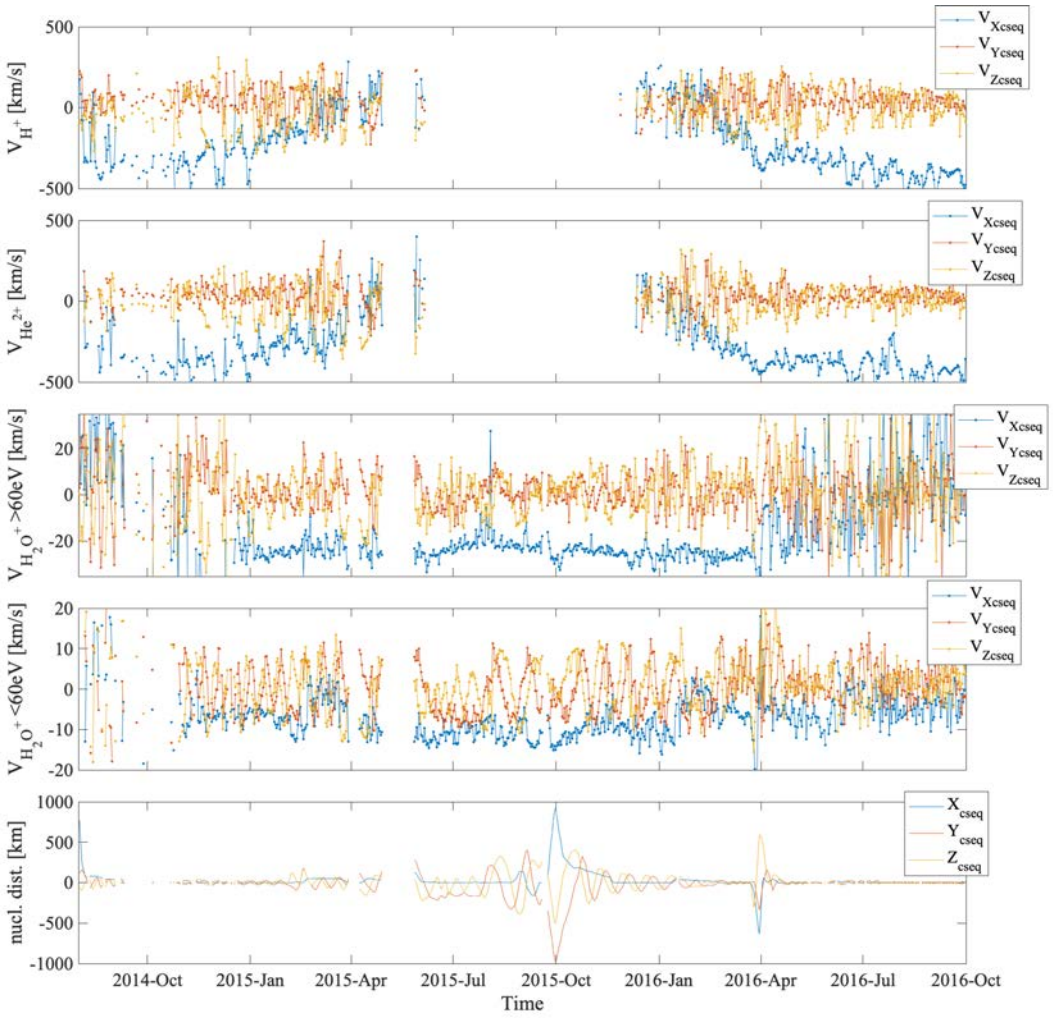

Figure 18 Velocity moments of ICA data (4 upper panels) and position of Rosetta relative to the nucleus (lowest panel). The velocity moemnts panels show from the top H^+, He^{2+}, H_2O^+ (assumed) above 60 eV and in the fourth panel below 60 eV. This data is now published in Nilsson et al. (2020).

The protons and alpha particles flow mainly in the anti-sunward direction (negative V_x) in the beginning and end of the active mission, as can be expected. In the middle of the active mission there is an absence of significant solar wind ions, the solar wind ion cavity. Just around the solar wind ion cavity the dominating solar wind ion flow is sunward (positive V_x), in agreement with the results reported by Behar et al. (2017) and Nilsson et al. (2017).
During most of the mission the cometary ions are predominantly flowing anti-sunward. Notable exceptions are seen in the above 60 eV cometary ions, which are frequently seen flowing sunward in the very early and late phases of the active mission. Some of this sunward flow is likely real, some more dubious. Inspection of the early sunward flow, observed in 2014, shows that this appears to be all due to enhanced noise levels in this data.

Another notable aspect in the cometary ion data for energies below 60 eV is the regular pattern of the V_y and V_z components. These changes follow the orbit of the spacecraft around the nucleus. It results from the low energy cometary ions

moving radially away from the nucleus in the Y-Z CSEQ plane, as reported in Bercic et al. (2018) and consistent with the cometary ion flow reported in Nilsson et al. (2015, 2017).
We can therefore conclude that the flow directions behave much according to previous reports using the full data set. This is the main reason why we have decided to split the cometary ion moments into two energy regions, below and above 60 eV.

For an example of where there may be problems with the data in general, and the moment data in particular, we will now look at an example and see how we can work with and judge the moment data by looking up specific features in the full data set. We begin with showing moments of cometary ions in the energy range above 60 eV from a few days around 1 May 2016, this time with no averaging, in Figure 20.

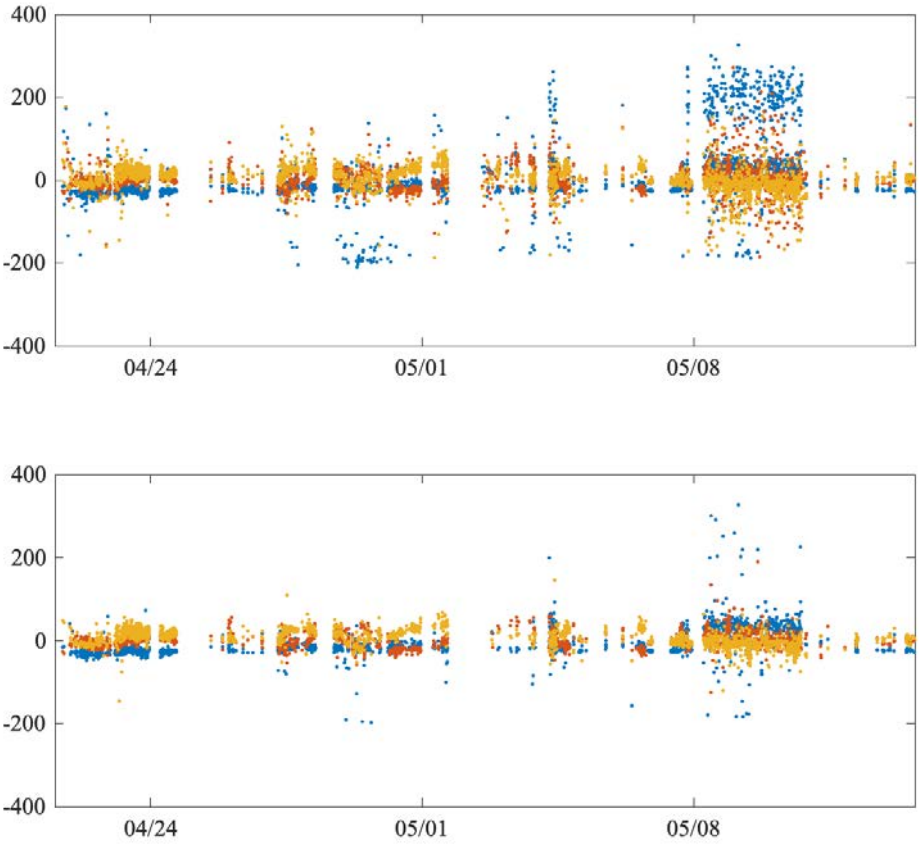

Figure 19 Ion flow for some days around 1 May 2016. The upper panel contains all data, the lower one has been filtered with the demand that the density is more than 0.001 cm^{-3}.

The upper panel shows all data. One can see that on 29 and 30 April there are data points with an x component of about –200 km/s. Inspection of energy spectrograms, mass spectrograms and azimuth – elevation distribution indicates that this is due to some cross-talk from He^+. The signal is very weak. Putting in a

demand that the density of this data set is above 0.001 cm^{-3} removes most of this signal, as seen in the lower panel of Figure 20. One can also notice a large amount of data points with an x component of about 200 km/s starting from 8 May. There appear to be large scatter in this data. A useful way of investigating the details is to look at the sector distribution of the signals. This is shown in Figure 21.

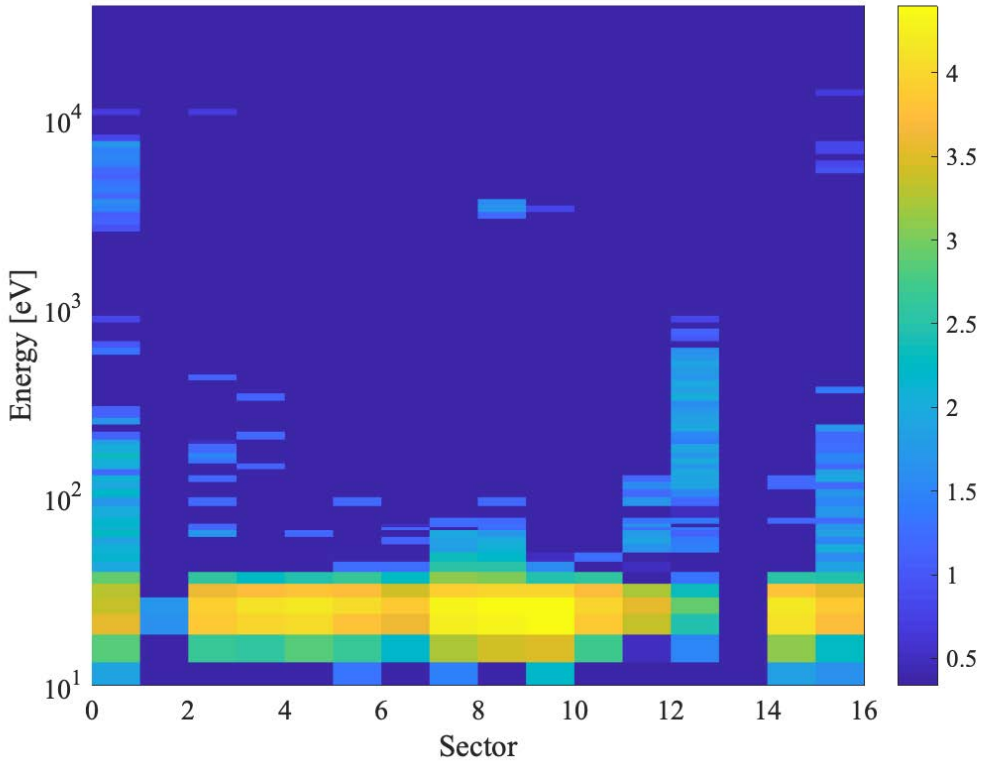

Figure 20 Colour coded energy spectrograms as function of sector. The colour scale indicates log_{10} summed counts.

There is a low energy signal centred on sector 8, extending also to somewhat higher energies. There is also a signal in sector 12 which is the usual higher energy cometary ion signal. There is also significant signal in sectors 0 and 15. This is common during this part of the mission. The signal at a few keV for sector 0 does not appear to be cross-talk from He+, an inspection of the He^+ energy spectrogram indicates a narrower energy range for He^+.

Using a threshold on the density of 0.001 cm^{-3} removes most of the higher velocity signal, and a lower speed with still sunward flow dominates. Thus this is dominated by the signal in sectors 0 and 15. It is possible that this signal is real, just as the signal at a few keV. In general, if a signal deviates strongly from what is seen most of the time, like a sunward flow, check the shape of the energy spectra, check the angular distribution (just sector distribution is often sufficient) to make sure that what looks like a signal in the moment data is not in fact just noise or cross-talk.

The above example also shows a major drawback with using moments. There are clearly several separate populations observed simultaneously. The best way to deal with these would be to separate them in energy and angular space and

calculate several moments. In the PSA data we have just made a rough energy division at 60 eV for cometary ions

Weak signals can always give unreliable velocity estimates, there is always some noise in the data which in the absence of a significant real signal can lead to spurious velocity estimates. Setting a lower density threshold of typically 0.001 to 0.01 cm^{-3} is therefore often a good idea. Integration of the moments should then also be performed by adding flux (n*V) and dividing with the sum of the density, to give little weight to weak signals.

Comparison with the RPC-LAP instrument

As part of the enhanced archive effort, the RPC-ICA omnidirectional flux (related to the density estimate above) has been compared to the ion current and spacecraft potential derived from the RPC-LAP data. From this study it is clear that there is a problem with the RPC_ICA densities for low energies. This is currently being investigated and is likely related to a problem with the RPC-ICA geometric factor at low energy combined with the extra limited field-of-view at low energies. Possibly the somewhat sparse energy scale at low energy also matters. For any future studies comparing RPC-ICA and RPC-LAP (and in practice RPC-MIP) it is worthwhile to look at time periods when the two instrument data sets show good co-variation. We therefore provide a flag that indicates when the RPC-ICA and RPC-LAP data have a correlation coefficient above 0.7. In practice this means that there are several peaks and larger scale slopes that match between the instruments. The correlation used was calculated over three hour intervals.

In Appendix 2 we show a brief report on the cross-correlation between the two data sets, performed with varying time windows. Examples are shown and it is discussed how the correlation flags can be used.

References

Behar, E., **H. Nilsson**, G. Stenberg Wieser, Z. Nemeth, T. W. Broiles, and I. Richter, Mass loading at 67P/Churyumov-Gerasimenko: A case study, Geophys. Res. Lett., 43, doi:10.1002/2015GL067436, 2016

E. Behar, H. Nilsson, M. Alho, C. Goetz, B. Tsurutani, The birth and growth of a solar wind cavity around a comet - Rosetta observations, Monthly Not. Roy. Astr. Soc., 469, S396 – S403, 2017

L Bercic, E Behar, H Nilsson, G Nicolaou, G Stenberg Wieser, M Wieser, C Goetz, Cometary ion dynamics observed in the close vicinity of comet 67P/Churyumov–Gerasimenko during the intermediate activity period, doi:10.1051/0004-6361/201732082, 2018

Nilsson, H., R. Lundin, K. Lundin, S. Barabash, H. Borg, O. Norberg, A. Fedorov, J.-A. Sauvaud, H. Koskinen, E. Kallio, P. Riihelä, J.-L. Burch, RPC-ICA: The Ion

Composition Analyzer of the Rosetta Plasma Consortium, Space Sci. Rev., doi: 10.1007/s11214-006-9031-z,2007

Nilsson, H., G. Stenberg Wieser, E. Behar, C. Simon Wedlund, H. Gunell, M. Yamauchi, R. Lundin, S. Barabash, M. Wieser, C. Carr, E. Cupido, J. L Burch, A. Fedorov, J.-A. Sauvaud, H. Koskinen, E. Kallio, J.-P. Lebreton, A. Eriksson, N. Edberg, R. Goldstein, P. Henri, C. Koenders, P. Mokashi, Z. Nemeth, I. Richter, K. Szego, M. Volwerk, C. Vallat, M. Rubin, Birth of a comet magnetosphere: A spring of water ions, Science, 347, 6220, doi: 10.1126/science.aaa0571, 2015

Nilsson, H., G. Stenberg Wieser, E. Behar, C. Simon Wedlund, E. Kallio, H. Gunell, N. Edberg, A. I. Eriksson, M. Yamauchi, C. Koenders, M. Wieser, R. Lundin, S. Barabash, K. Mandt, J. L. Burch, R. Goldstein, P. Mokashi, C. Carr, E. Cupido, P. T. Fox, K. Szego, Z. Nemeth, A. Fedorov, J.-A. Sauvaud, H. Koskinen, I. Richter, J.-P. Lebreton, P. Henri, M. Volwerk, C. Vallat, B. Geiger, Evolution of the ion environment of comet 67P/Churyumov-Gerasimenko – Observations between 3.6 and 2.0 AU, Astronomy and Astrophysics, http://dx.doi.org/10.1051/0004-6361/201526142, 2015

Hans Nilsson, Gabriella Stenberg Wieser, Etienne Behar, Herbert Gunell, Martin Wieser, Marina Galand, Cyril Simon Wedlund, Markku Alho, Charlotte Goetz, Masatoshi Yamauchi, Pierre Henri, Elias Odelstad, Erik Vigren; Evolution of the ion environment of comet 67P during the Rosetta mission as seen by RPC-ICA, Monthly Notices of the Royal Astronomical Society, Volume 469, Issue Suppl_2, 21 July 2017, Pages S252–S261, https://doi.org/10.1093/mnras/stx1491

C Simon Wedlund, E Kallio, M Alho, H Nilsson, G Stenberg Wieser, H Gunell, E Behar, J Pusa, G Gronoff, The atmosphere of comet 67P/CG diagnosed by charge-exchanged solar wind alpha particles, Astronomy and Astrophysics, doi: 10.1051/0004-6361/201527532, 2015

C. Simon Wedlund, E. Behar, H. Nilsson, M. Alho, E. Kallio, H. Gunell, D. Bodewits, K. Heritier, M. Galand, A. Beth, M. Rubin, K. Altwegg, G. Gronoff, R. Hoekstra, Solar wind charge exchange in cometary atmospheres. III. Results from the Rosetta mission to comet 67P/Churyumov-Gerasimenko, Astronomy and Astrophysics, doi:10.1051/0004-6361/201834881, 2019

Gabriella Stenberg Wieser, Elias Odelstad, Martin Wieser, Hans Nilsson, Charlotte Goetz, Tomas Karlsson, Mats André, Leif Kalla, Anders I Eriksson, Georgios Nicolaou, Cyril Simon Wedlund, Ingo Richter, and Herbert Gunell, Investigating short time-scale variations in cometary ions around comet 67P, Monthly Not. Roy. Astr. Soc., 469, S522-S534, 2017

Appendix 1

Content of L2 PSA data

The data files consist of 10 positions with information and then 8, 32 or 96 positions with an energy spectrum depending on the number of energy steps in the data. In the PDS table the latter 8 to 96 positions are in one column. The data file columns are described in words below. The same information is found in the data label. The number of rows is variable.

Column

1. Start time of the observations in Universal Time
2. Delta T, duration of the observation in seconds
3. Quality flags, 8 positions where 0 means no known problem, x means not implemented for this data set. The flags are described in section 3.3 in the EAICD.
4. Instrument mode, gives the instrument binning mode as a number between 8 and 31. See instrument paper or User Guide for interpretation.
5. Noise reduction. The number of counts subtracted on board from each data point (after binning).
6. Mass table used. ICA may use mass look-up tables on board to bin data into certain physical mass ranges (see section 2.4.3). This column describes which of three on-board tables was used. 0 indicates that no mass look-up table was used, 1 indicates the table for no post-acceleration (reference value 0), 2 low post acceleration (reference value 1-4) and 3 high post-acceleration (reference value 5-7).
7. Post-acceleration reference level (0-7). Necessary to know in order to interpret the mass channels correctly in terms of physical mass of measured particles
8. Azimuth index (0-15). See sections 2, 2.4.3 and figures 2 and 3 in the EAICD.
9. Elevation index (0-15) See sections 2, 2.4.3 and figures 2 and 3 in the EAICD.
10. Mass channel number (0-31).
11. Count-values for the different energy steps in the energy spectrogram. The energy levels are found in the file ICA_ENERGY_TABLE_VNN.LBL in the CALIB directory.

Content of L3 PSA data

The data files consist of 10 positions with information and then 8, 32 or 96 positions with an energy spectrum depending on the number of energy steps in the data. . In the PDS table the latter 8 to 96 positions are in one column. The data file columns are described in words below. . The same information is found in the data label. The number of rows is variable. The format is identical to L2 data except for the unit of the data which is differential flux [particles / s / cm^2 / sr / eV].

Column

1. Start time of the observations in Universal Time
2. Delta T, duration of the observation in seconds
3. Quality flags, 8 positions where 0 means no known problem, x means not implemented for this data set. The flags are described in section 3.3.
4. Instrument mode, gives the instrument binning mode as a number between 8 and 31. See instrument paper or User Guide for interpretation.
5. Noise reduction. The number of counts subtracted on board from each data point (after binning).
6. Mass table used. ICA may use mass look-up tables on board to bin data into certain

physical mass ranges (see section 2.4.3). This column describes which of three on-board tables was used. 0 indicates that no mass look-up table was used, 1 indicates the table for no post-acceleration, 2 low post acceleration and 3 high post-acceleration.
7. Post-acceleration reference level (0-7). Necessary to know in order to interpret the mass channels correctly in terms of physical mass of measured particles. Which mass table to use for a certain post-acceleration reference value is given in the file "ICA_POST_ACC_TABLE_V02.LBL" in the CALIB directory.
8. Azimuth index (0-15). See sections 2, 2.4.3 and figures 2 and 3.
9. Elevation index (0-15) See sections 2, 2.4.3 and figures 2 and 3.
10. Mass channel number (0-31).
11. Differential flux [particles / s / cm^2 / sr / eV] flux for the different energy steps in the energy spectrogram. The energy levels are found in the file ICA_ENERGY_TABLE_VNN.LBL in the CALIB directory.

Content of L4 CORR PSA data

The data files consist of 10 positions with information and then 8, 32 or 96 positions with an energy spectrum depending on the number of energy steps in the data. . In the PDS table the latter 8 to 96 positions are in one column. The data file columns are described in words below. . The same information is found in the data label. The number of rows is variable. The format is identical to the L3 data. The data format is described in the label files and summarised below. In addition there is a ZERO file containing the confidence interval of the zero level. Values less than the value in the ZERO file cannot be considered significantly different from zero. The L4 CORR CTS data set follows the same layout, but the data is in counts instead of differential flux.

Format of data file:

Column
1. Start time of the observations in Universal Time
2. Delta T, duration of the observation in seconds
3. Quality flags, 8 positions where 0 means no known problem, x means not implemented for this data set. The flags are described in section 3.3.
4. Instrument mode, gives the instrument binning mode as a number between 8 and 31. See instrument paper or User Guide for interpretation.
5. Noise reduction. The number of counts subtracted on board from each data point (after binning).
6. Mass table used. ICA may use mass look-up tables on board to bin data into certain physical mass ranges (see section 2.4.3). This column describes which of three on-board tables was used. 0 indicates that no mass look-up table was used, 1 indicates the table for no post-acceleration, 2 low post acceleration and 3 high post-acceleration.
7. Post-acceleration reference level (0-7). Necessary to know in order to interpret the mass channels correctly in terms of physical mass of measured particles. Which mass table to use for a certain post-acceleration reference value is given in the file "ICA_POST_ACC_TABLE_V02.LBL" in the CALIB directory.
8. Azimuth index (0-15). See sections 2, 2.4.3 and figures 2 and 3.
9. Elevation index (0-15) See sections 2, 2.4.3 and figures 2 and 3.
10. Mass channel number (0-31).
11. And onward: contains differential flux [particles / s / cm^2 / sr / eV] flux for the different energy steps in the energy spectrogram. The energy levels are found in the file ICA_ENERGY_TABLE_VNN.LBL in the CALIB directory.

Format of ZERO file:

1. Start time of the observations in Universal Time

2. Azimuth index (0-15). See sections 2, 2.4.3 and figures 2 and 3.
3. Elevation index (0-15) See sections 2, 2.4.3 and figures 2 and 3.
4. Mass channel number (0-31).
5. “uncertainty value”. Data values less than this value cannot be considered significantly different from zero.

Content of L4 PHYS-MASS PSA data

The data files consist of 8 positions with information and then 8, 32 or 96 positions with an energy spectrum depending on the number of energy steps in the data. . In the PDS table the latter 8 to 96 positions are in one column. The data file columns are described in words below. The same information is found in the data label. The number of rows is variable. The format is similar to L3 data, but each ion mass range is provided in a separate file, and no mass table or mass channel information is given in the data. The files are named
RPCICAYYYYMMDDTHH_xxx_L4_I
where I can be H, HE2, HE or HVY for ion masses of 1,2,4 and more than 16 amu respectively. Apart from the indicated ion mass the file naming convention is the same as for the other data sets. Thus xxx is a running file number allowing for several files for the same time, each with a different software version of the data obtained within a one hour time interval. The data format is described in the label files and summarised below.

Column

1. Start time of the observations in Universal Time
2. Delta T, duration of the observation in seconds
3. Quality flags, 8 positions where 0 means no known problem, x means not implemented for this data set. The flags are described in section 3.3.
4. Instrument mode, gives the instrument binning mode as a number between 8 and 31. See instrument paper or User Guide for interpretation.
5. Noise reduction. The number of counts subtracted on board from each data point (after binning).
6. Post-acceleration reference level (0-7). Necessary to know in order to interpret the mass channels correctly in terms of physical mass of measured particles. Which mass table to use for a certain post-acceleration reference value is given in the file “ICA_POST_ACC_TABLE_V02.LBL” in the CALIB directory.
7. Azimuth index (0-15). See sections 2, 2.4.3 and figures 2 and 3.
8. Elevation index (0-15) See sections 2, 2.4.3 and figures 2 and 3.
9. Differential flux [particles / s / cm^2 / sr / eV] flux for the different energy steps in the energy spectrogram. The energy levels are found in the file ICA_ENERGY_TABLE_VNN.LBL in the CALIB directory.

Content of L2 Geometry PSA data

The geometry files contain geometry data with a suitable temporal resolution for the corresponding ICA data. The files contain the position of the comet relative to the Sun, the position of the spacecraft relative to the comet and the orientation of the spacecraft. The reference frame used is J2000 and the coordinate system Comet Sun Equatorial (CSEQ) where X points towards the Sun, Z along the spin axis of the Sun and Y completes a right-handed system. The data format is described in the label files.

The GEOM data design consists of a table with 9 columns containing the following information:

Column

1. Time (UTC)

2. Distance to Sun, X,Y,Z in ECLIPJ2000 coordinates in km

3. Distance to target in km, X.Y,Z in 67P/C-G_CSEQ coordinate system for the main target 67P

4. Velocity relative to current target in km/s

5. Distance to surface of current target (altitude) in km

6. Latitude on surface of current target in degrees

7. Longitude on surface of current target in degrees

8. Speed relative to current target in km/s

9. Spacecraft attitude expressed as unit vectors for spacecraft X,Y,Z expressed in the local target coordinate system (e.g. 67P/C-G_CSEQ)

Content of L2 Housekeeping PSA data

The housekeeping data is retained in the archive mainly for completeness. The generally useful parameters provided are the instrument and sensor temperatures. In particular the sensor temperature can affect the instrument performance. The sensor temperature form the basis for one of our quality flags, see section 3.3. The temperatures are given as calibrated values [°C].

All other housekeeping data concern mainly commands, modes and reference and monitor values for different voltages on-board. The reference and monitor values are provided as digital reference values, not calibrated values. Calibration information is found in the ICA_TABLES document provided in the DOCUMENTS directory of the data set. The data format is described in the label files.

The HK data design consists of a table with 42 columns containing the following information:

1. Time, UTC
2. Instrument mode
3. Instrument SID (Telemetry rate, see instrument paper)
4. Instrument sensor temperature, calibrated value °C
5. Instrument DPU temperature, calibrated value °C
6. Micro channel plate (MCP) main 28V switch on/off (0/1)
7. Opto main 28 V switch on/off (0/1)
8. Main 28 V switch on/off (0/1)
9. Post-acceleration high voltage on/off (0/1)
10. Grid low voltage on / off (0/1)
11. Entrance high voltage on/off (0/1)
12. Deflection low voltage on/off (0/1)
13. Deflection high voltage on/off (0/1)
14. MCP high voltage present (0/1)
15. Opto 28 V present (0/1)
16. Main 28 V present (0/1)
17. Opto monitor value (digital reference value 0-255)

18. MCP monitor value (digital reference value 0-255)
19. Deflection high voltage monitor (digital reference value 0-255)
20. Deflection low voltage monitor (digital reference value 0-255)
21. Post acceleration high voltage monitor (digital reference value 0-255)
22. Grid low voltage monitor (digital reference value 0-255)
23. Entrance upper high voltage monitor (digital reference value 0-511)
24. Entrance lower high voltage monitor (digital reference value 0-511)
25. Energy deflection high voltage reference (digital reference value 0-4095)
26. Energy deflection low voltage reference (digital reference value 0-4095)
27. Entrance upper reference value (digital reference value 0-4095)
28. Grid reference value (digital reference value 0-7)
29. MCP high voltage current reference (digital reference value 0-15)
30. Opto high voltage current reference (digital reference value 0-15)
31. MCP high voltage default reference ((digital reference value 0-7)
32. Opto high voltage default reference ((digital reference value 0-7)
33. Post acceleration low level reference (digital reference value 0-7)
34. Post acceleration high level reference (digital reference value 0-7)
35. Post acceleration level low / high (0/1)
36. Post acceleration mode fixed / alternating (0/1)
37. Last command status (0-3, with 0 ok)
38. New command received toggle bit (0/1)
39. First word command return (0-65525)
40. Direct command switch (0/1)
41. FIFO filling in terms of internal packets (0 – 20000)
42. FIFO overflow (0-255)

Content of L5 Moment data

The moment data is contained in one file with velocity and density moments for H^+, He^{2+}, He^+ and water ions (assumed mass in moment calculations). The data contains the assumed mass and charge. The cometary ion (water) moments are divided into two energy ranges, <= 60 eV and > 60 eV.

Column
1. Start time of the observations in Universal Time
2. Species, can be 1=H, 2=He2, 3=He, 4=H2O (<=60eV), 5=H2O (>60eV)
3. Mass, can be 1,2,4 and 18
4. Charge, in unit charges, can be 1 and 2
5. Density, cm^{-3}, number density
6. Vx component, [km/s] in the CSEQ frame
7. Vy component, [km/s] in the CSEQ frame
8. Vz component, [km/s] in the CSEQ frame
9. Duration, the length of the complete measurement cycle
10. Quality flags, 8 positions where 0 means no known problem, x means not implemented for this data set. The flags are described in section 3.3 in the EAICD

Appendix 2

Summary of ICA _LAP cross-calibration

The flags are derived from three lists of starting times of 3-hour windows when ICA total ion flux data and LAP data of 1) P1 ion flux ('ci'), 2) spacecraft potential ('cu') and 3) derived local plasma density ('ce') have correlation coefficients higher than 0.7, from 20140801 to 20160930. This report discusses the correlation between the RPC-ICA omnidirectional flux and the RPC-LAP ion current, spacecraft potential and density derived from the spacecraft potential. As the latter is a derivation of the spacecraft potential, it is not used in the RPC-ICA archive flags.

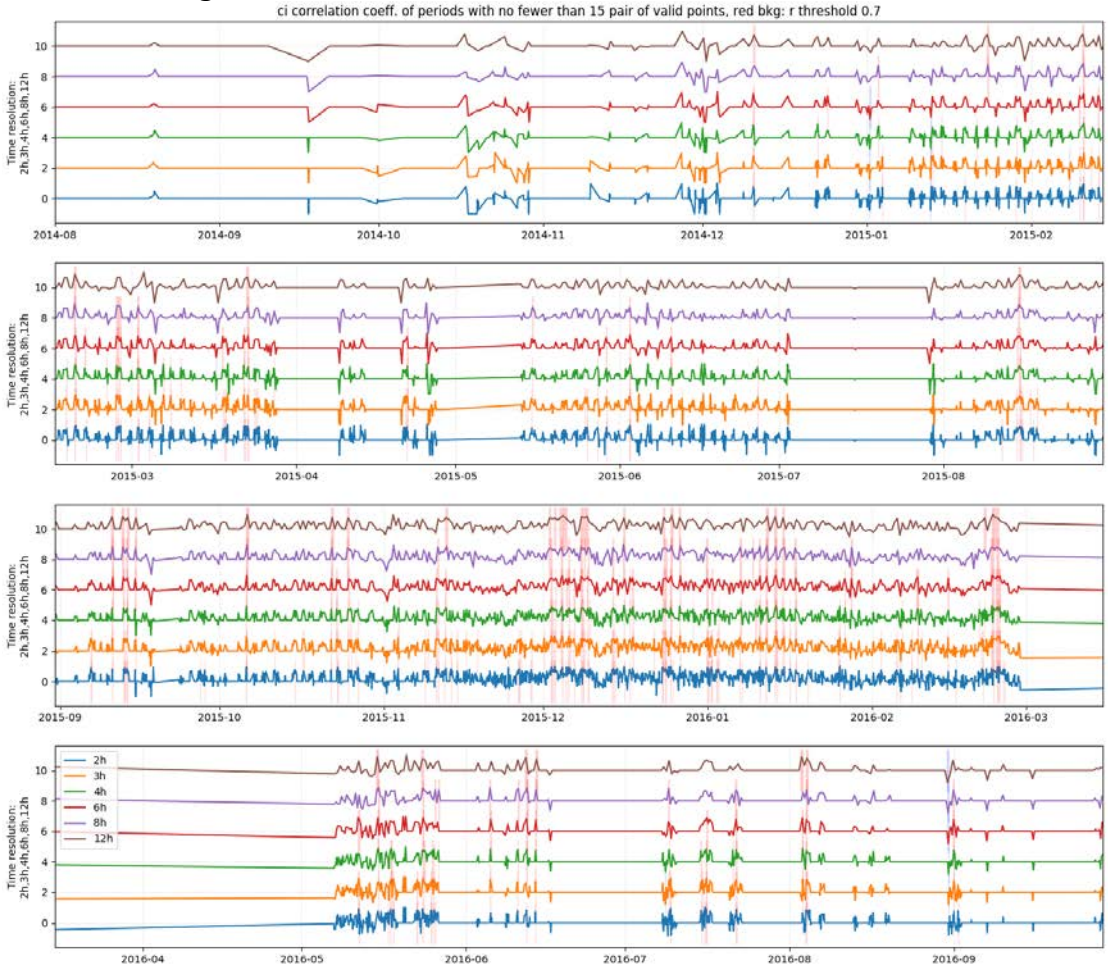

Figure A 21: Correlation coefficient (rc) between ICA ion flux (fc) and LAP ion flux derived from LAP ion current measurements (i1L). Each line shows the rc within a time window of a fixed length. We tested different window lengths (2h, 3h, 4h, 6h, 8h, 12h), and selected the 3-hour window for the correlation flags. The pink stripes mark the period when the rc is higher than 0.7, i.e., the flagged periods.

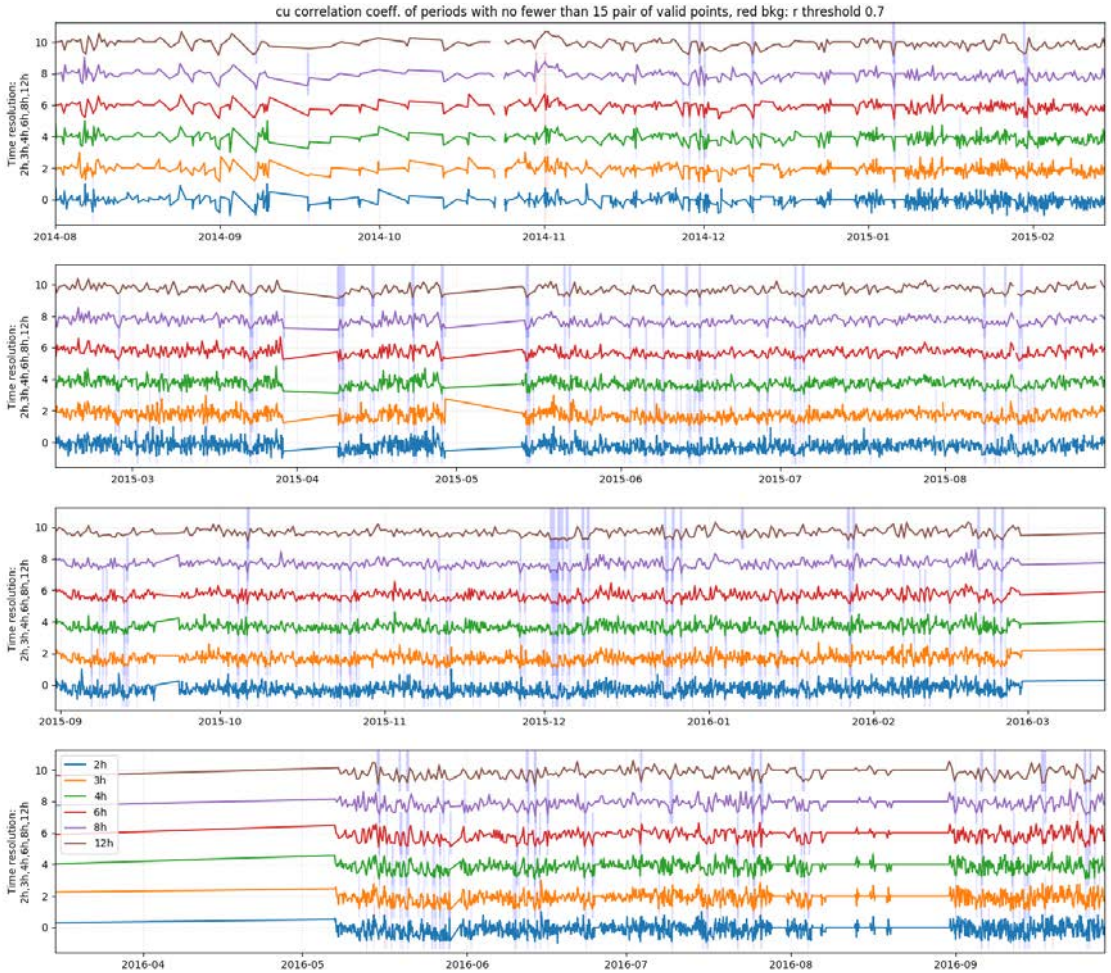

Figure A22: Similar figure to Figure A 21 but for the correlation between fc and the spacecraft potential (Usc) measured by LAP. The periods where rc is lower than -0.7 are shown as blue shades because an anti-correlation is expected between fc and Usc.

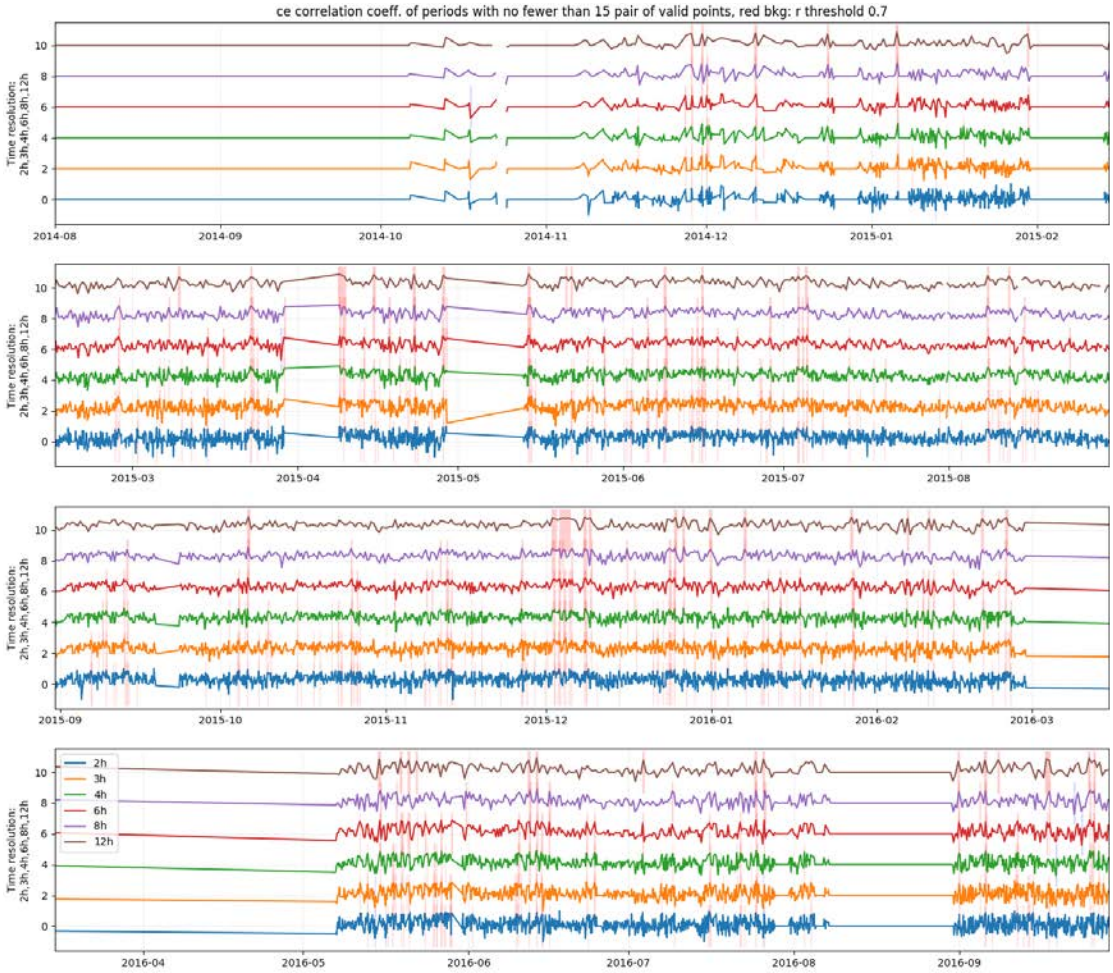

Figure A 23: Similar to Figure A 21 but for the correlation between fc and the local plasma density (Ne) derived from Usc.

Correlated quantities

ICA total ion flux (*fc*)

The total ion flux measured by all energy bins and all directions covered by ICA, in the unit of [$cm^{-2}\ s^{-1}$]. *fc* contains ions of both solar wind and cometary origins. The processing procedure to derive *fc* DOES contain

1. Correction of ICA's known instrumental artifacts.
2. Unification of different direction binning schemes used in different modes.
3. Unification of different energy tables used in different modes.
4. Differential flux conversion using energy, species and post-acceleration-dependent geometric factors.

The processing procedure to derive *fc* DOES NOT contain

1. Spacecraft potential correction.
2. Correction of performance variation due to ICA temperature variation.
3. Compensation for incomplete directional coverage, therefore if most of the particles come from the blocked directions, the total flux would be underestimated.
4. Compensation for incomplete energy coverage, e.g., very low energies for cometary ions.

LAP data

Three LAP data products are used for comparison and correlation with *fc*:

1. Ion current measured by LAP Probe 1, *i1L*. Its correlation with *fc* is abbreviated as 'ci' hereafter.
2. Spacecraft potential, *Usc*. Its correlation with *fc* is abbreviated as 'cu' hereafter.
3. Local plasma density *Ne,* derived from *Usc*. Its correlation with *fc* is abbreviated as 'ce' hereafter.

The *i1L* data are adopted from the LAP archived dataset. The data files come from directories with the name RO-C-RPCLAP-5-yymm-DERIV-V0.8, where yymm are the two-digit numbers for year and month. Only files with '_I1L' endings in the names are used. These files are the ion current values measured in working modes with a fixed sweeping voltage. The ion currents in *i1L* data are in the unit of [ampere]. We converted it to ion flux f_L = *i1L / qe / Aeff*, where *qe* =1.602e-19 [C] is the element charge, *Aeff = pi * 2.5 * 2.5 [cm^2]* is the assumed effective area of LAP probe 1.

The *Usc* values are derived with LAP measurements in two modes:

1. In the sweeping mode, the *Usc* is defined as the zero-crossing of the current in the sweep, analogous to the floating probe potential.
2. In the electric field mode, the *Usc* is the 32-second average of 3 volts minus the measured potential of LAP probe 1.

The *Ne* data are the plasma charge density in the unit of [cm^{-3}]. It has been empirically cross-calibrated with MIP density. The *Ne* is derived from *Usc*, therefore they are almost always anti-correlated.

How to use the flags

The correlation flags are three lists of UTC times, corresponding to *fc*'s correlations with LAP ion current *i1L* ('ci'), LAP spacecraft potential *Usc* ('cu'), and derived plasma density *Ne* ('ce'), respectively.

Each UTC marks the beginning of a 3-hour-long window during which *fc* was well correlated with one of the three LAP quantities. Here the "well correlated" means that *fc* and the LAP quantity show somewhat co-variation. Numerically, it is defined as the correlation coefficients greater than 0.7.

Figure A 24 shows an example of a flagged period of good correlation between ICA *fc* and all LAP quantities. The solid blue curves are the time series of the respective quantity. The red dotted curves are the logarithms of the ratio between ICA ion flux and the blue curve in the current panel, with the scales on the vertical axis to the right. Panels d, f and h show the linear regression results (green lines) of ICA ion flux versus the *i1L, Usc* and *Ne*, respectively. One can see the co-variation of *fc* and all LAP quantities during this window period. Note that for *Usc*, an anticorrelation is expected. The correlation is further quantified by the correlation efficiency, which is ~0.92 in this case. This event is a demonstration of the effectiveness of the correlation coefficiency in identifying good correlation events.

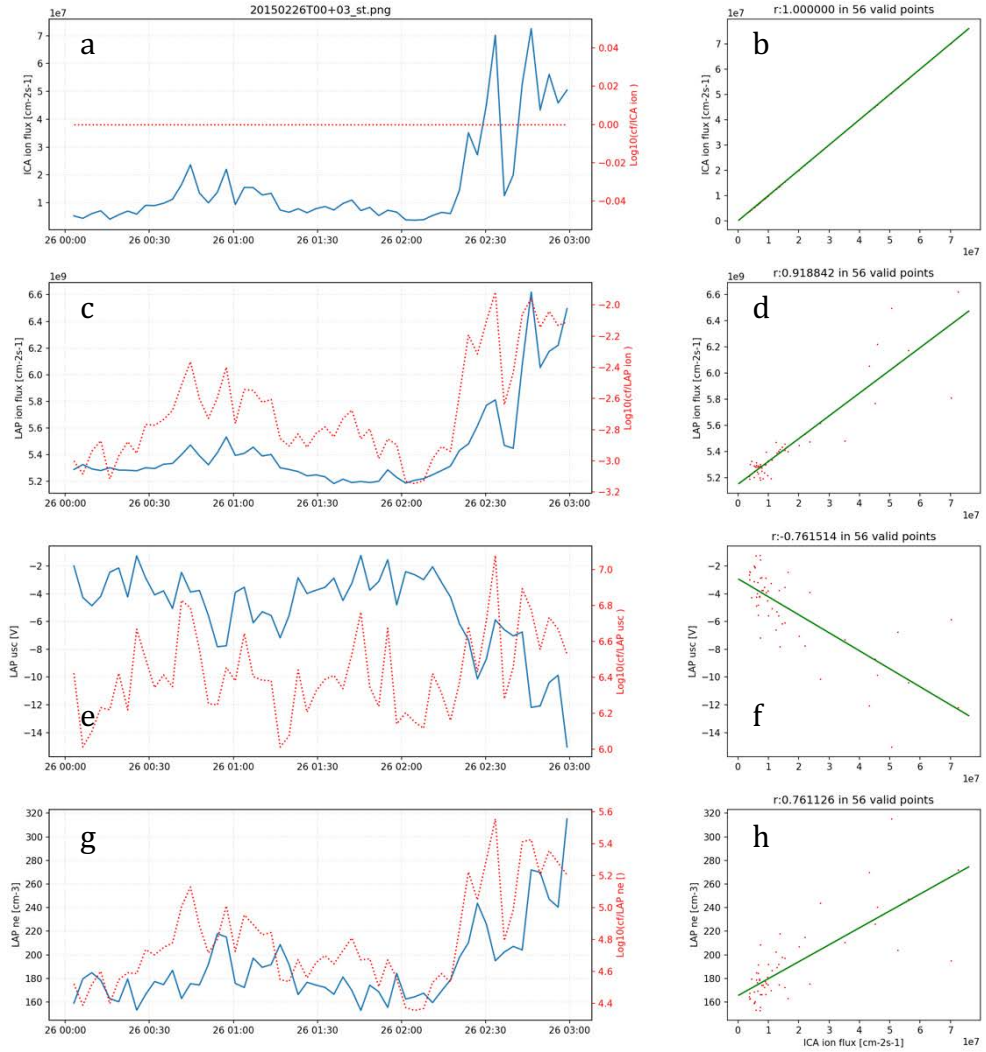

Figure A 24: An example of a good correlation event. The ICA ion flux (a) is well correlated with all LAP quantities: (c) i1L, (e) Usc and (g) Ne. The solid blue curves are the time series of the respective quantity. The red dotted curves are the logarithms of the ratio between ICA ion flux and the blue curve in the current panel whose scales are on the right-hand side vertical axis. Panels d, f and h show the linear regression results (green line) of ICA ion flux versus i1L, Usc and Ne, respectively. This is a rare event when all three LAP quantities are well correlated (rc > 0.7) with ICA ion flux.

The flags should be used to identify periods of relatively good correlation between *fc* and LAP quantities, *i1L, Usc* and *Ne*. For a more detailed study, the user must look at the original data of all measurements.

Sample correlation study

We picked out all ICA and LAP data when the correlations ci, cu and ce as defined above were higher than 0.7.

All the data during well correlated *cf* and *i1L* are shown in figure A 5.:In figure A 6 we have instead used a demand for good correlation *cf* and *Usc*. In the final figure we show the correlation between cf and the LAP density estimate derived from the spacecraft potential.
From the figures we can see that the ICA current appears to be 2 to 3 orders of magnitude smaller than the LAP ion current. We can also see that the dynamic range of the LAP ion current is rather small. The original idea was to compare with the LAP ion current as this should be the most similar physical property measured by the two instruments. Instead it turns out that the spacecraft potential and the density derived form it are more useful.
Clearly more work must be done on the cross-calibration of the low energy ICA data. We know from case studies that at times the similarity can be quite good (see figure 15). A comparison of the RPC-LAP (and/or MIP) density with the RPC-ICA density for the whole mission together with the co-variation flag should help us identify when and where the ICA density estimates are good and how we can correct the density estimates at the lowest energies to improve the RPC_ICA density estimate. We show a time series of the ICA and LAP densities in our final figure, from which suitable time periods

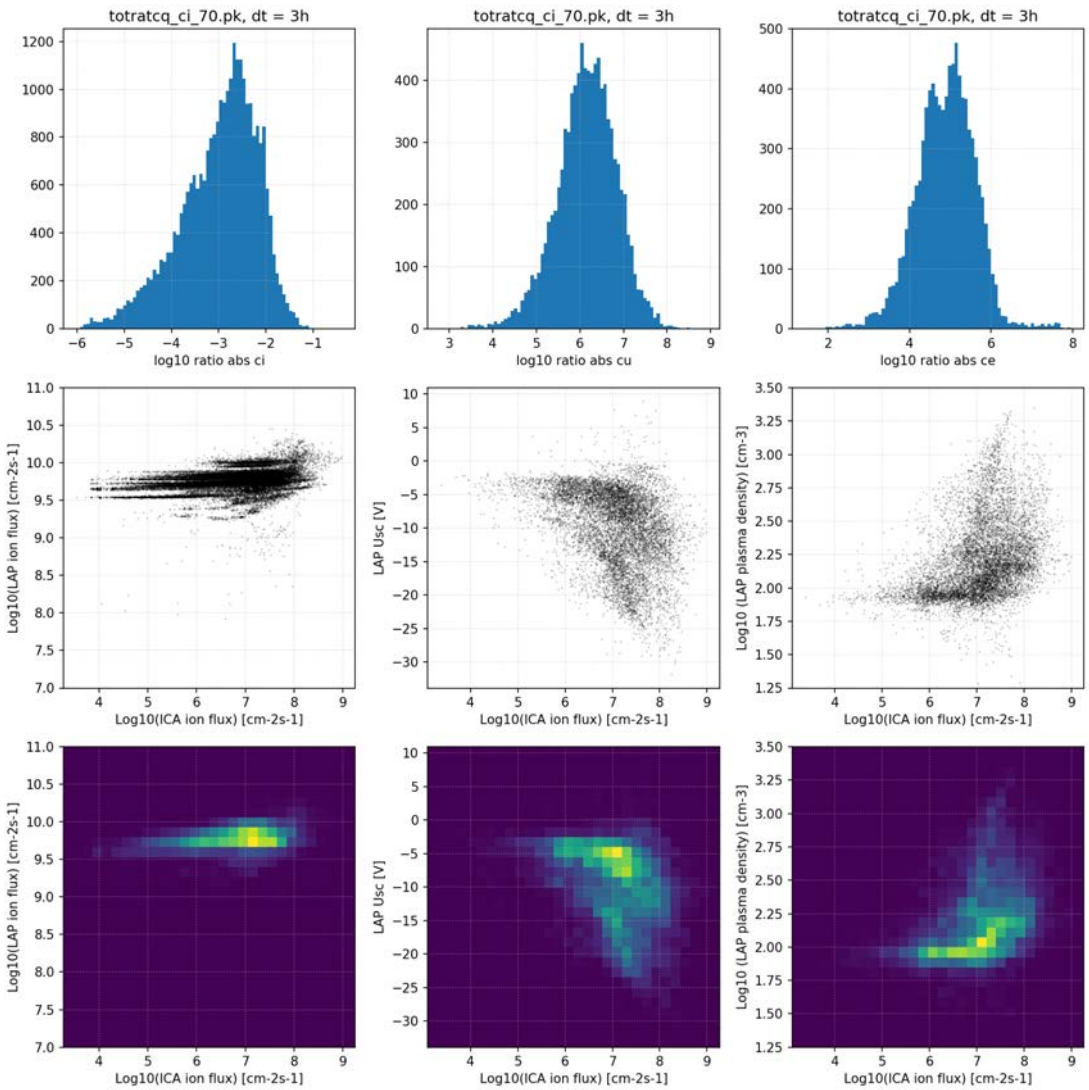

Figure A 25: Statistics of data during good correlation between cf and i1L. Columns from left to right are associated with LAP ion current/flux data, LAP spacecraft potential data, and LAP plasma density data, respectively. Rows from top to bottom: histogram of the log10(ratio of ICA ion flux over the absolute value of the quantity associated with current column), scatter plot of the current quantity vs. ica ion flux, and the histogram of the scatter plot.

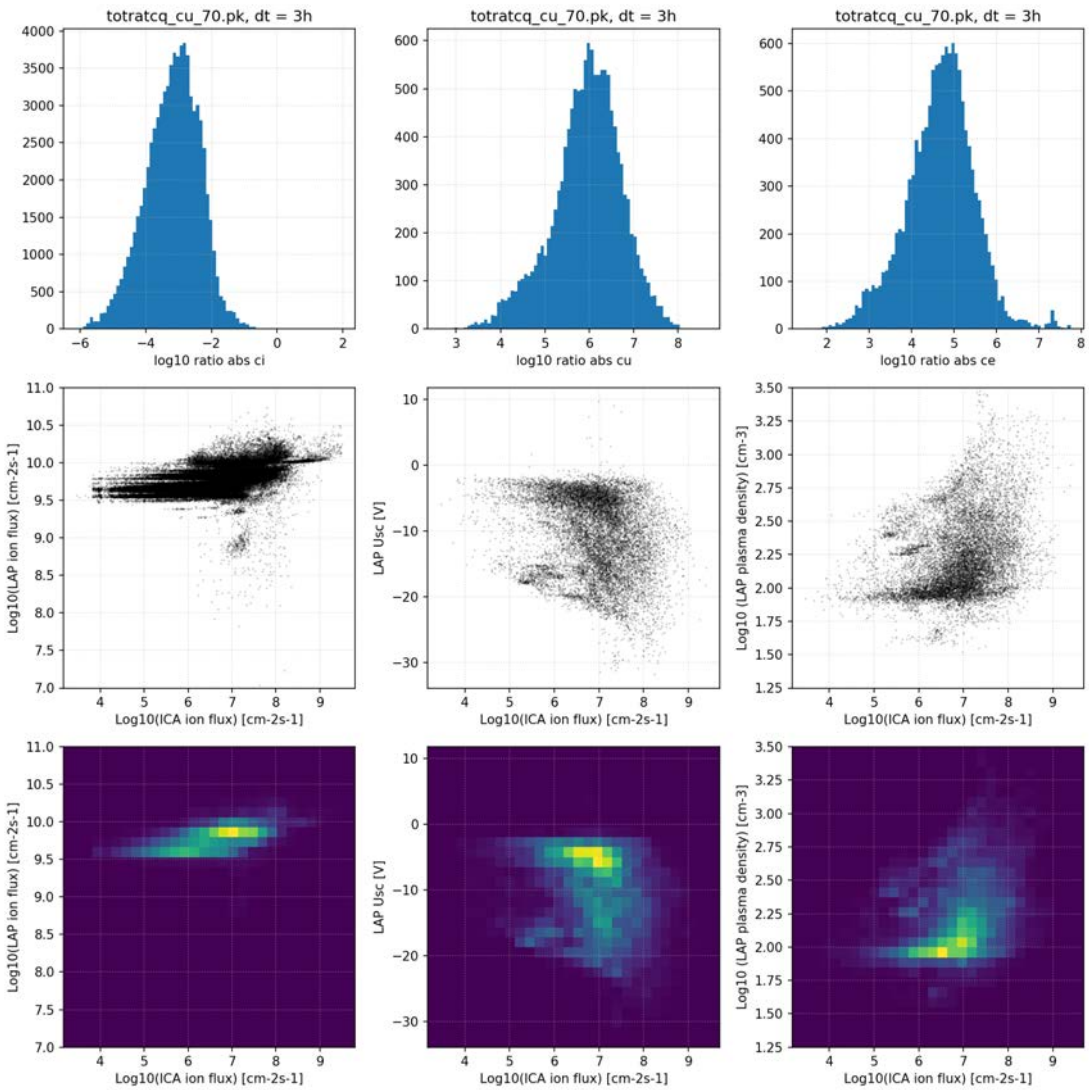

Figure A 26: Similar to Figure A 25 but for data when the correlation between ICA ion flux and LAP spacecraft potential is good.

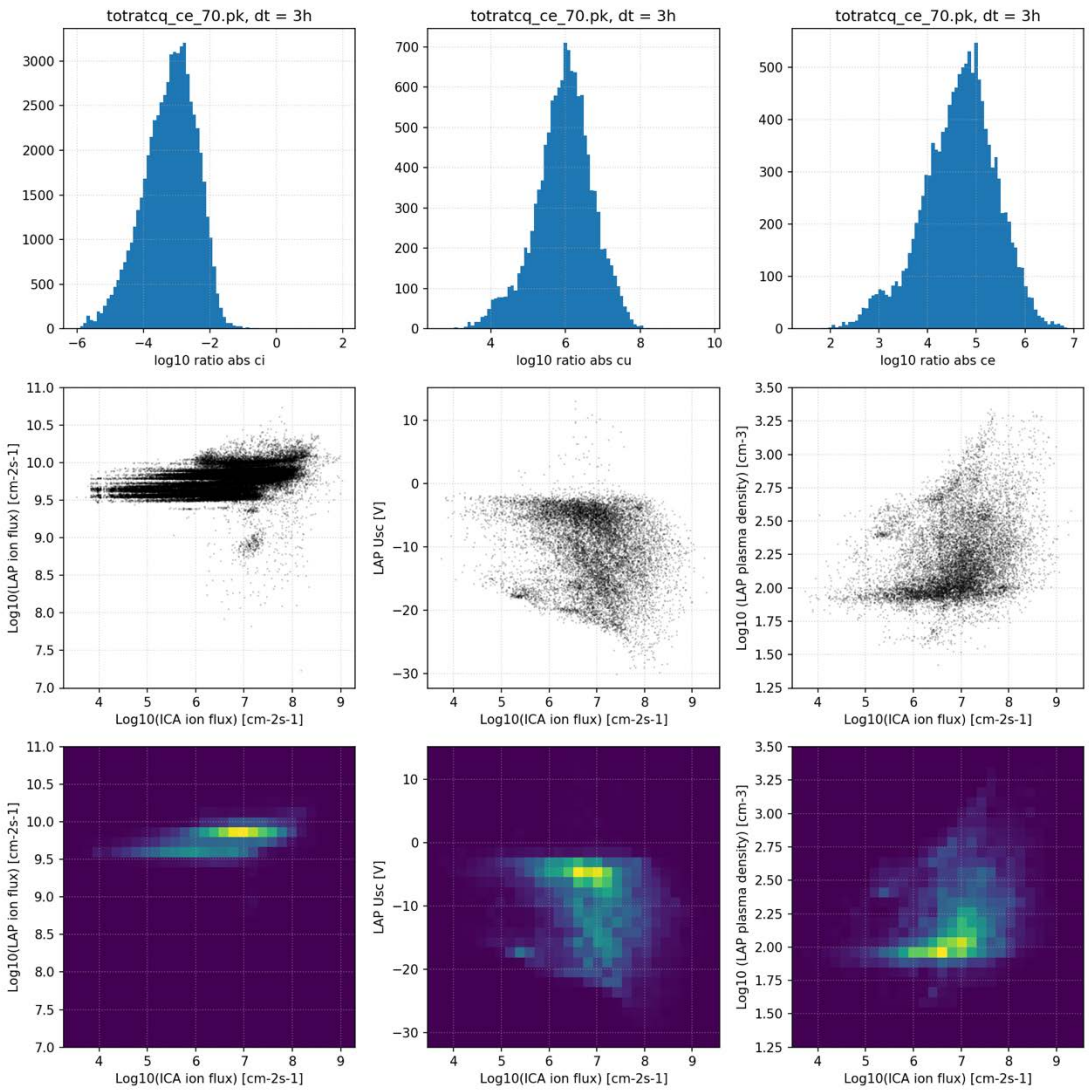

Figure A 7 : Similar to Figure A 25 but for data when the correlation between ICA ion flux and the LAP density estimate is good.

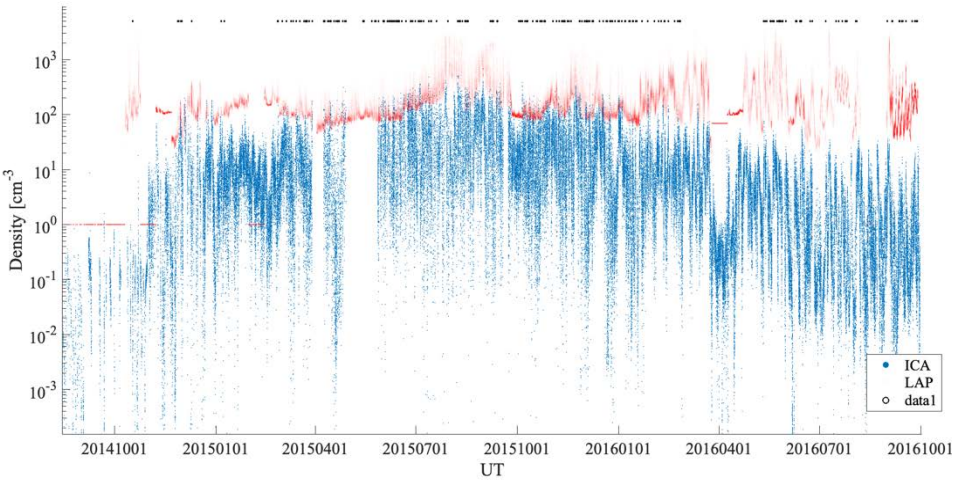

Figure A 8: LAP (red) and ICA (blue) density estimates. Times with good co-variation on a 3 hour time scale is indicated with a block dot in the top of the plot.